Nonequilibrium phonon effects on transport properties through atomic and molecular bridge junctions

Yoshihiro Asai
Research Institute for Computational Sciences (RICS), National Institute of Advanced Industrial Science and Technology (AIST), Umezono 1-1-1, Tsukuba Central 2, Tsukuba, Ibaraki 305-8568, Japan
and CREST, Japan Science and Technology Corporation (JST), Kawaguchi 332-0012, Japan
(Received 12 November 2007; revised manuscript received 22 May 2008; published 31 July 2008)

We have studied nonequilibrium phonon effects on the electric current and the energy current through atomic and molecular bridge junctions in terms of the Su-Schrieffer-Heeger model. Due to the inelastic coupling between electrons and phonons, the two currents are closely correlated. The correlation was taken into account in our theory where kinetic equations are solved not only for electrons but also for phonons. The offset behavior of the inelastic tunneling spectrum is successfully described by our theory. In addition to this, it was found that a vibronic energy current arises as a result of the inelastic coupling and a nonequilibrium phonon effect, similar to the phonon drag effect, even in isothermal conditions.

DOI: 10.1103/PhysRevB.78.045434 PACS number(s): 81.07.Nb, 73.63.−b, 68.37.Ef, 72.10.−d

I. INTRODUCTION

Ballistic electron transport is generally expected to exist in nanoscale objects, whose length is much shorter than its mean free path.[1,2] Its realization in both atomic wires and molecular wires has been anticipated, which is one of the reasons why molecular electronics[3–16] is expected to open a new door in quantum computation.

Recent experimental studies of atomic wires and single molecular bridge junctions, however, have provided some results which do not always justify this anticipation.[17–24] With the help of theoretical developments in calculating vibronic currents, including both the elastic and the inelastic-scattering effects of electrons in these systems,[25–52] it has been found that electron-phonon or electron-intramolecular-vibration couplings are necessary to explain the main features of the experimental results.[17–24] Details of the vibronic currents in atomic wires and single molecular bridge junctions, for example, the line shape[49–52] of the voltage dependence of d^2I/dV^2 and the vibrational mode dependence,[38–40,47,48] have recently become subjects of intense investigations. Nonetheless, many problems still remain to be solved in further detail.

Even in the most elaborate theoretical models, heat dissipation accompanying the electronic current have not been taken into account.[38–40,53] In bridge-junction theories, electrons are allowed to be thermalized only in electrodes, while electrons in atomic wires or molecules are exposed to nonequilibrium conditions. On the other hand, atomic wire phonons or molecular vibrations are kept isolated from the thermalized phonons in the electrodes. Moreover, they are assumed to be in direct contact with the heat bath, and hence, they are in a thermally equilibrium state. Therefore electronic energy dissipated into atomic wire phonons or molecular vibrations are readily absorbed into the heat bath without being transferred to the electrodes. In this model, electron transport and phonon energy transport are not necessarily consistent with each other. Thus, the model includes some unphysical features which should be elaborated upon.

Here, we develop a theory where both electron transports and energy transports are calculated self-consistently. The two couplings, i.e., the mechanical coupling between the atomic wire phonons (the molecular vibrations) and the thermalized phonons in the electrodes, as well as the coupling between the atomic wire phonons (the molecular vibrations) and the electron-hole excitations, are taken into account in the calculations. Both of these give rise to energy damping pathways for the wire phonons or molecular vibrations. Thus, our theory includes the influence of the nonequilibrium phonon (molecular vibration) on the vibronic current.

With this theoretical setup, we will discuss the heat dissipation pathways accompanying the electronic current in isothermal conditions. We have found that a vibronic energy current component appears as a result of the inelastic-scattering effect and the nonequilibrium phonon effect. We have also found that the offset appears in the voltage dependence of d^2I/dV^2, as well as that it depends on the voltage, the energy, and the link force field. The offset is important for characterizing the global current-voltage (I-V) behavior at higher-voltage regions. We also discuss the vibrational mode dependency of the vibronic response of the electronic current and investigate the conditions for which ballistic transport is realized in these systems.

II. THEORY

A. Bridge-shaped junction

An atomic or single molecular bridge junction is composed of a conductor (an atomic chain or a single molecular chain) and two electrodes. The conductor is linked to each electrode through a single bond, i.e., the terminal atom of the conductor is located on the top site of the surface. Here, the electrode is assumed to have the face center cubic (fcc) structure, and the surface of the electrode is assumed to be (001). Moreover, the lattice constant is denoted by a. The above model represents the bridge-junction system whose electron transport and energy transport we study below.

We adopt the Su-Schrieffer-Heeger (SSH) model[54] to describe the electron and the ionic motion in the bridge junction;

$$H = -\sum_{\langle ij\rangle,\beta,\sigma} t_{ij}[1-\lambda_{ij}^{\beta}(u_{i\beta}-u_{j\beta})](c_{i\sigma}^{\dagger}c_{j\sigma}+\text{H.c.}) + \sum_{i,\sigma}\varepsilon_i n_{i\sigma} + 1/2\sum_{j=1}^{N}\sum_{\beta=1}^{3} M_j(du_{j\beta}/dt)^2 + U(\vec{r}_1,\vec{r}_2,\ \ldots,\vec{r}_N), \tag{1}$$

where $U(\vec{r}_1,\vec{r}_2,\cdots,\vec{r}_N)$ and $\vec{r}_j$ denote the N-body atomic potential and the atomic position vector of the jth atom, respectively, and $u_{j\beta}$ denotes the βth Cartesian component of the displacement vector $\vec{u}_j$, which is given by $\vec{u}_j=\vec{r}_j-\vec{R}_j$. Moreover, $\vec{R}_j$ and M_j represent the equilibrium position vector and the mass of the jth atom, and σ, $c_{j\sigma}^{\dagger}(c_{j\sigma})$, and $n_{j\sigma}$ denote the spin variable, the creation (annihilation) operator of the electron with spin σ at the jth atom, and its corresponding number operator. Furthermore, t_{ij}, λ_{ij}^{β}, and ε_i denote the transfer integral between the ith and the jth atoms, the electron-phonon coupling constant between the ith and the jth atoms along the β direction, and the site energy of the ith atom. Also, $\langle ij\rangle$ implies that the summation over the atomic site is limited to the nearest-neighbor pairs, where N denotes the number of atoms.

We take into account the electron-phonon coupling only within the conductor and at the link between the conductor and the electrodes. The contribution of the transversal phonon modes to the coupling is ignored,

$$\lambda_{ij}^{\beta} = \begin{cases} \lambda & i,j \in \text{conductor} \quad \beta = z \\ \lambda & i \in \text{conductor} \quad j \in \text{electrode} \quad \beta = z \\ \lambda & i \in \text{electrode} \quad j \in \text{conductor} \quad \beta = z \\ 0 & \text{otherwise}. \end{cases}$$

We also assume that the transfer integral and the site energy are uniform in the conductor and the electrodes,

$$t_{ij} = \begin{cases} t & i,j \in \text{conductor} \\ t_M & i,j \in \text{electrode} \\ t_L & i \in \text{conductor} \quad j \in \text{electrode} \\ t_L & i \in \text{electrode} \quad j \in \text{conductor}, \end{cases}$$

$$\varepsilon_i = \begin{cases} \varepsilon & i \in \text{conductor} \\ \varepsilon_M & i \in \text{electrode}. \end{cases}$$

B. Classical phonons

We first discuss the classical phonon Hamiltonian H_{ph}.[55,56] The N-body potential can be written as a sum of two-body potentials $\phi(\vec{r})$; $U(\vec{r}_1,\vec{r}_2,\cdots,\vec{r}_N)=1/2\Sigma_{i,j}\phi(\vec{r}_i-\vec{r}_j)$. Up to the second order of $u_{j\alpha}$, the potential can be given approximately by $U(\vec{r}_1,\vec{r}_2,\cdots,\vec{r}_N)=1/2\Sigma_{i,j=1}^{N}\Sigma_{\alpha,\beta=1}^{3}(u_{i\alpha}u_{i\beta}-u_{i\alpha}u_{j\beta})\,(\partial^2\phi\partial r_\alpha\partial r_\beta)|_{\vec{R}_i-\vec{R}_j}$. Then, we have the following Hamiltonian:

$$H_{\text{ph}} = 1/2\sum_{j=1}^{N}\sum_{\alpha=1}^{3} M_j(du_{j\alpha}/dt)^2 + 1/2\sum_{ij}^{N}\sum_{\alpha\beta}^{3} u_{i\alpha}\Phi_{\alpha\beta}(\vec{R}_i-\vec{R}_j)u_{j\beta}, \tag{2a}$$

where

$$\Phi_{\alpha\beta}(0) = \sum_{k}^{N} \left.\frac{\partial^2\phi}{\partial r_\alpha\,\partial r_\beta}\right|_{\vec{R}_i-\vec{R}_k} \qquad \Phi_{\alpha\beta}(\vec{R}_i-\vec{R}_j) = -\left.\frac{\partial^2\phi}{\partial r_\alpha\,\partial r_\beta}\right|_{\vec{R}_i-\vec{R}_j} (i\neq j). \tag{2b}$$

In some cases, it might be useful to work with the mass-weighted displacement rather than the displacement itself, i.e., $\vec{\xi}_j=\sqrt{M_j}\vec{u}_j$. Then, the Hamiltonian can be written as follows:

$$H_{\text{ph}} = 1/2\sum_{j=1}^{N}\sum_{\alpha=1}^{3}(d\xi_{j\alpha}/dt)^2 + (1/2)\sum_{ij}^{N}\sum_{\alpha\beta}^{3}\xi_{i\alpha}K_{\alpha\beta}(\vec{R}_i-\vec{R}_j)\xi_{j\beta}, \tag{2c}$$

$$K_{\alpha\beta}(\vec{R}_i-\vec{R}_j) = \frac{\Phi_{\alpha\beta}(\vec{R}_i-\vec{R}_j)}{\sqrt{M_iM_j}}. \tag{2d}$$

The classical equation of motion for the mass-weighted displacement $\xi_{i\alpha}$ is thus given by $d^2\xi_{i\alpha}dt^2=-\Sigma_{j=1}^{N}\Sigma_{\beta=1}^{3}K_{\alpha\beta}(\vec{R}_i-\vec{R}_j)\xi_{j\beta}$. If we introduce the Fourier component of the displacement, i.e., $\xi_{j\alpha}(t)=\xi_{j\alpha}e^{-i\omega t}$, the equation of motion is now written as follows:

$$\omega^2\xi_{i\alpha} - \sum_{j=1}^{N}\sum_{\beta=1}^{3}K_{\alpha\beta}(\vec{R}_i-\vec{R}_j)\xi_{j\beta} = 0. \tag{3}$$

For the sake of simplicity, we adopt the Lennard-Jones potential for $\phi(\vec{r})$ and impose the nearest-neighbor cutoff for the potential;

$$\begin{cases} \phi(\vec{r}) = A(r_0r)^{12} - 2A(r_0r)^6 & r \le r_{\text{nn}} \\ \phi(\vec{r}) = 0 & r > r_{\text{nn}}, \end{cases} \tag{4}$$

where $r=|\vec{r}|$. r_0 and r_{nn} are the equilibrium and the nearest-neighbor distances, respectively. By definition, the gradient of the Lennard-Jones potential is zero at the equilibrium distance. By choosing $r_{\text{nn}}=r_0$, we avoid the need for numerical optimizations to find the stable structure, i.e., the stable structure of our system is obtained by constructing piles of stable dimmers.

Later we will discuss the bridge-junction structure which comprises the conductor and the electrodes and display nonuniform and complex behavior. For this purpose, it will be convenient to specify the position indices in the force field $K_{\alpha\beta}(i,j)$, $\Phi_{\alpha\beta}(i,j)$ or $K_{\alpha\beta}(\vec{R}_i;\vec{R}_j)$, $\Phi_{\alpha\beta}(\vec{R}_i;\vec{R}_j)$ rather than their original expressions in terms of the distance: $K_{\alpha\beta}(\vec{R}_i-\vec{R}_j)$ and $\Phi_{\alpha\beta}(\vec{R}_i-\vec{R}_j)$.

C. Quantum phonons

Next, we quantize the classical phonons of our bridge-junction system. For this purpose, we calculate their retarded Green's function in real space directly without introducing the normal coordinate prior to the calculation. Let us start by defining the retarded Green's function in terms of the correlation function of the mass-weighted displacements,[57]

$$D^R_{\alpha,\beta}(i,j;t) = \langle\langle \xi_{i\alpha}(t); \xi_{j\beta}(0)\rangle\rangle = -i\theta(t)\langle[\xi_{i\alpha}(t), \xi_{j\beta}(0)]\rangle. \tag{5}$$

The Fourier transform is denoted as follows:

$$D^R_{\alpha,\beta}(i,j;\omega) = \frac{1}{2\pi}\int_{-\infty}^{\infty} D^R_{\alpha,\beta}(i,j;t)e^{i\omega_+ t}dt = \langle\langle \xi_{i\alpha}; \xi_{j\beta}\rangle\rangle_\omega, \tag{6}$$

where $\omega_+ = \omega + i\eta$ and η represents a small positive number. The equation of motion for the retarded Green's function is then given by

$$i\partial_t D^R_{\alpha,\beta}(i,j;t) = \delta(t)\langle[\xi_{i\alpha}, \xi_{j\beta}]\rangle + \theta(t)\langle[\partial_t \xi_{i\alpha}(t), \xi_{j\beta}(0)]\rangle. \tag{7}$$

It should be noted that any i which is not placed in a superscript or a subscript denotes the pure imaginary unit. ∂_t denotes the first-order partial derivative with respect to t. Now we use the commutation relations between the displacement and the momentum variables to achieve the canonical quantization in the process of solving the equation of motion.[57] The first term on the right-hand side of Eq. (7) disappears due to the commutation relation between the displacement variables $[\xi_{i\alpha}, \xi_{j\beta}]=0$. By using the Heisenberg equation,

$$\partial_t \xi_{i\alpha}(t) = -\frac{i}{\hbar}[\xi_{i\alpha}(t), H_{\rm ph}] = p_{i\alpha}(t), \tag{8}$$

where $p_{i\alpha}$ denotes the momentum, the equation of motion for the retarded Green's function is modified to yield

$$i\partial_t D^R_{\alpha,\beta}(i,j;t) = i\langle\langle p_{i\alpha}(t); \xi_{j\beta}(0)\rangle\rangle \equiv iC^R_{\alpha,\beta}(i,j;t). \tag{9}$$

The Fourier transform of the retarded Green's function is therefore expressed in terms of the dynamical momentum-displacement correlation function,

$$D^R_{\alpha,\beta}(i,j;\omega) = \frac{i}{\omega_+}\langle\langle p_{i\alpha}; \xi_{j\beta}\rangle\rangle_\omega = \frac{i}{\omega_+}C^R_{\alpha,\beta}(i,j;\omega). \tag{10}$$

Similarly, the equation of motion for $C^R_{\alpha,\beta}(i,j;t)$ is given by

$$\begin{aligned} i\partial_t C^R_{\alpha,\beta}(i,j;t) &= \delta(t)\langle[p_{i\alpha}, \xi_{j\beta}]\rangle + \theta(t)\langle[\partial_t p_{i\alpha}(t), \xi_{j\beta}(0)]\rangle \\ &= -i\hbar\delta_{ij}\delta_{\alpha\beta}\delta(t) + \frac{1}{\hbar}\langle\langle [p_{i\alpha}(t), H_{\rm ph}]; \xi_{j\beta}(0)\rangle\rangle, \end{aligned} \tag{11}$$

where the commutation relation between the momentum and the displacement variable $[p_{i\alpha}, \xi_{j\beta}] = -i\hbar\delta_{ij}\delta_{\alpha\beta}$ and the Heisenberg equation $\partial_t p_{i\alpha}(t) = -i\hbar[p_{i\alpha}(t), H_{\rm ph}]$ are used for the second term on the right-hand side of Eq. (11). The Fourier transform of $C^R_{\alpha,\beta}(i,j;t)$ is then given by

$$C^R_{\alpha,\beta}(i,j;\omega) = \frac{-1}{\omega_+}\left\{\frac{i\hbar}{2\pi}\delta_{ij}\delta_{\alpha\beta} - \frac{1}{\hbar}\langle\langle [p_{i\alpha}, H_{\rm ph}]; \xi_{j\beta}\rangle\rangle_\omega\right\}. \tag{12}$$

By using Eq. (1), $[p_{i\alpha}(t), H_{\rm ph}]$ is given by

$$[p_{i\alpha}(t), H_{\rm ph}] = -i\hbar\sum_{j\lambda} K_{\alpha\lambda}(i,j)\xi_{j\lambda}(t), \tag{13}$$

where $K_{\alpha\beta}(i,j) \equiv K_{\alpha\beta}(\vec{R}_i - \vec{R}_j)$. In deriving Eq. (13), we have used $[p_{i\alpha}(t), H] = e^{iHt}[p_{i\alpha}, H_{\rm ph}]e^{-iHt}$ and the symmetry condition for the potential, i.e.,

$$K_{\alpha\beta}(i,j) = K_{\beta\alpha}(j,i). \tag{14}$$

Equation (13) helps us to evaluate $\langle\langle [p_{i\alpha}, H_{\rm ph}]; \xi_{j\beta}\rangle\rangle_\omega$,

$$\begin{aligned} \langle\langle [p_{i\alpha}, H_{\rm ph}]; \xi_{j\beta}\rangle\rangle_\omega &= -i\hbar\sum_{k\lambda} K_{\alpha\lambda}(i,k)\langle\langle \xi_{k\lambda}; \xi_{j\beta}\rangle\rangle_\omega \\ &= -i\hbar\sum_{k\lambda} K_{\alpha\lambda}(i,k)D^R_{\lambda,\beta}(k,j;\omega). \end{aligned} \tag{15}$$

Thus, we obtain the following expression of $C^R_{\alpha,\beta}(i,j;\omega)$:

$$C^R_{\alpha,\beta}(i,j;\omega) = \frac{-i}{\omega_+}\left\{\frac{\hbar}{2\pi}\delta_{ij}\delta_{\alpha\beta} + \sum_{k\lambda} K_{\alpha\lambda}(i,k)D^R_{\lambda,\beta}(k,j;\omega)\right\}. \tag{16}$$

By combining Eqs. (10) and (16), we obtain the following representation of the equation of motion for the retarded phonon Green's function, which is defined by Eq. (6),

$$\sum_{k\lambda}\{\omega_+^2\delta_{ki}\delta_{\lambda\alpha} - K_{\alpha\lambda}(i,k)\}D^R_{\lambda,\beta}(k,j;\omega) = \frac{\hbar}{2\pi}\delta_{\alpha\beta}\delta_{ij}. \tag{17}$$

The corresponding retarded phonon Green's function can be defined for the non mass-weighted displacement $\vec{u}_j$,

$$\tilde{D}^R_{\alpha,\beta}(i,j;t) = \langle\langle u_{i\alpha}(t); u_{j\beta}(0)\rangle\rangle, \tag{18}$$

Similarly, it is given by

$$\sum_{k\lambda}\{M_k\omega_+^2\delta_{ki}\delta_{\lambda\alpha} - \Phi_{\alpha\lambda}(i,k)\}\tilde{D}^R_{\lambda,\beta}(k,j;\omega) = \frac{\hbar}{2\pi}\delta_{\alpha\beta}\delta_{ij}. \tag{19}$$

The advanced phonon Green's functions $D^A_{\alpha,\beta}(i,j;\omega)$ and $\tilde{D}^A_{\alpha,\beta}(i,j;t)$ are given by the complex conjugates of $D^R_{\alpha,\beta}(i,j;\omega)$ and $\tilde{D}^R_{\alpha,\beta}(i,j;t)$. The merit of the equation of motion method discussed here is that the calculation is performed entirely without using the eigenstate of the system. In fact, the method has been applied successfully for systems where the symmetry is broken, such as the mass impurity problem in solids, etc.[57] This is a great advantage especially to our problem, where the calculation of the eigenstate of semi-infinite electrodes linked to a conductor is difficult to perform due to the infinite dimensions of the electrode. In an alternative method which we adopt in the following, we only need the surface phonon Green's function and the phonon Green's function of the conductor. By combining the two Green's functions, it is possible to calculate the phonon Green's function of the whole system, which will be described later.

In dividing the whole mechanical system into electrodes and conductor regions, we assume that the Lennard-Jones

parameters depend on the region where the potential is defined, i.e., $A=A_C$, $r_0=a_C$ in the conductor, $A=A_M$, $r_0=a_M$ in the electrode, and $A=A_L$, $r_0=a_L$ on the link, where a_C and a_L are the interatomic distance in the conductor and the link, respectively, and a_M is the lattice constant in the electrode. The force field parameter $k=144A/r_0^2$ is introduced for each region, i.e., $k_C=144A_C/a_C^2$, $k_M=144A_M/a_M^2$, and $k_L=144A_L/a_L^2$. Likewise, the ionic mass M_j depends on the region where the ion is located, i.e., $M_j=M_C$ when $j \in$ conductor and $M_j=M_M$ when $j \in$ electrode.

D. Surface phonon Green's function of the electrode

In principle, the phonon Green's function equations in Eqs. (17) and (19) apply both for the conductor and the electrodes. However, it might be useful to take into account the two-dimensional translational symmetry of the electrode in the calculations.[55,58,59] Our bridge-junction system is divided into two electrode parts and a conductor part. Accordingly, the number of atoms is divided such that $N=2N_M+N_C$, where N_M and N_C denote the number of atoms in the electrode and the conductor, respectively. Although the electrode is assumed to be semi-infinite along the positive or the negative branch of the z axis, it is periodic along the layer defined by the x and y axes, whose translational vector is denoted by $\vec{l}_\parallel$. The phonon Green's function equation for the electrode in Eq. (17) can be classified in terms of the two-dimensional wave vector $\vec{Q}_\parallel$ and the indexes specifying the principal layer in the electrode l_z, rather than the atomic position indexes i and j,

$$\sum_{l_z''\lambda} \{\omega_+^2 \delta_{l_z,l_z''} - K_{\alpha\lambda}(l_z,l_z'';\vec{Q}_\parallel)\} D^R_{\lambda,\beta}(l_z'',l_z';\vec{Q}_\parallel,\omega) = \frac{\hbar}{2\pi}\delta_{\alpha\beta}\delta_{l_z,l_z'}, \tag{20a}$$

$$K_{\alpha\beta}(l_z,l_z';\vec{Q}_\parallel) = \frac{1}{N_\parallel}\sum_{\vec{l}_\parallel,\vec{l}_\parallel'} K_{\alpha\beta}(\vec{l}_\parallel l_z;\vec{l}_\parallel' l_z') e^{-i\vec{Q}_\parallel\cdot\{\vec{R}(\vec{l}_\parallel l_z)-\vec{R}(\vec{l}_\parallel' l_z')\}}, \tag{20b}$$

$$D^R_{\alpha,\beta}(l_z,l_z';\vec{Q}_\parallel,\omega) = \frac{1}{N_\parallel}\sum_{\vec{l}_\parallel,\vec{l}_\parallel'} D_{\alpha\beta}(\vec{l}_\parallel l_z,\vec{l}_\parallel' l_z';\omega) e^{-i\vec{Q}_\parallel\cdot\{\vec{R}(\vec{l}_\parallel l_z)-\vec{R}(\vec{l}_\parallel' l_z')\}}, \tag{20c}$$

where $N_\parallel$ is the number of the two-dimensional unit cell. Now the phonon Green's function equation of our bridge-junction given in Eq. (17) is divided into two parts. One is the conductor part, which will be given later, and the other is the electrode part given in Eqs. (20a)–(20c). It should be pointed out that these two parts of the phonon Green's function couple through the potential and the displacement at the links, which will be discussed in Sec. II E. Using the matrix notation, Eq. (20a) can be written as follows:

$$\begin{pmatrix} \omega_+^2\mathbf{I}-\mathbf{K}_0(\vec{Q}_\parallel) & -\mathbf{K}_+(\vec{Q}_\parallel) & 0 & \cdots \\ -\mathbf{K}_-(\vec{Q}_\parallel) & \omega_+^2\mathbf{I}-\mathbf{K}_0(\vec{Q}_\parallel) & -\mathbf{K}_+(\vec{Q}_\parallel) & \cdots \\ 0 & & \ddots & \\ \vdots & & & \end{pmatrix} \times \begin{pmatrix} \mathbf{D}^R_{0,0}(\vec{Q}_\parallel,\omega) & \mathbf{D}^R_{0,1}(\vec{Q}_\parallel,\omega) & \cdots \\ \mathbf{D}^R_{1,0}(\vec{Q}_\parallel,\omega) & \mathbf{D}^R_{1,1}(\vec{Q}_\parallel,\omega) & \ddots \\ \vdots & & \end{pmatrix} = \frac{\hbar}{2\pi}\mathbf{I}_{3\mathbf{N}_L\times 3\mathbf{N}_L}, \tag{21}$$

where $\mathbf{I}$ and $\mathbf{I}_{3N_M\times 3N_M}$ are 3×3 and $3N_M\times 3N_M$ unit matrices, respectively. The matrix components of the supermatrices in Eq. (21) are summarized in Appendix A. Using Eqs. (21) and (A1)–(A4), we obtain the following relation, which is valid for $l_z \geq 1$:

$$\mathbf{D}^R_{l_z,0}(\vec{Q}_\parallel,\omega) = \tau_0(\vec{Q}_\parallel,\omega)\mathbf{D}^R_{l_z-1,0}(\vec{Q}_\parallel,\omega) + \tilde{\tau}_0(\vec{Q}_\parallel,\omega)\mathbf{D}^R_{l_z+1,0}(\vec{Q}_\parallel,\omega), \tag{22a}$$

$$\tau_0(\vec{Q}_\parallel,\omega) = \{\omega_+^2\mathbf{I}-\mathbf{K}_0(\vec{Q}_\parallel)\}^{-1}\mathbf{K}_+^\dagger(\vec{Q}_\parallel), \tag{22b}$$

$$\tilde{\tau}_0(\vec{Q}_\parallel,\omega) = \{\omega_+^2\mathbf{I}-\mathbf{K}_0(\vec{Q}_\parallel)\}^{-1}\mathbf{K}_+(\vec{Q}_\parallel), \tag{22c}$$

where we have used the fact that $\mathbf{K}_-=\mathbf{K}_+^\dagger$. By performing recursive substitutions on the left-hand side of Eq. (22a) into the two terms on the right-hand side of the same equation, the following relations are found to be satisfied:[60]

$$\mathbf{D}^R_{l_z,0}(\vec{Q}_\parallel,\omega) = \tau_1(\vec{Q}_\parallel,\omega)\mathbf{D}^R_{l_z-2,0}(\vec{Q}_\parallel,\omega) + \tilde{\tau}_1(\vec{Q}_\parallel,\omega)\mathbf{D}^R_{l_z+2,0}(\vec{Q}_\parallel,\omega), \tag{23a}$$

$$\tau_1(\vec{Q}_\parallel,\omega) = \{1-\tau_0(\vec{Q}_\parallel,\omega)\tilde{\tau}_0(\vec{Q}_\parallel,\omega) - \tilde{\tau}_0(\vec{Q}_\parallel,\omega)\tau_0(\vec{Q}_\parallel,\omega)\}^{-1}\tau_0(\vec{Q}_\parallel,\omega)^2, \tag{23b}$$

$$\tilde{\tau}_1(\vec{Q}_\parallel,\omega) = \{1-\tilde{\tau}_0(\vec{Q}_\parallel,\omega)\tilde{\tau}_0(\vec{Q}_\parallel,\omega) - \tilde{\tau}_0(\vec{Q}_\parallel,\omega)\tau_0(\vec{Q}_\parallel,\omega)\}^{-1}\tilde{\tau}_0(\vec{Q}_\parallel,\omega)^2. \tag{23c}$$

Using inductive arguments, we then obtain the following equations:

$$\mathbf{D}^R_{l_z,0}(\vec{Q}_\parallel,\omega) = \tau_1(\vec{Q}_\parallel,\omega)\mathbf{D}^R_{l_z-2^i,0}(\vec{Q}_\parallel,\omega) + \tilde{\tau}_1(\vec{Q}_\parallel,\omega)\mathbf{D}^R_{l_z+2^i,0}(\vec{Q}_\parallel,\omega), \tag{24a}$$

$$\tau_i(\vec{Q}_\parallel,\omega) = \{1-\tau_{i-1}(\vec{Q}_\parallel,\omega)\tilde{\tau}_{i-1}(\vec{Q}_\parallel,\omega) - \tilde{\tau}_{i-1}(\vec{Q}_\parallel,\omega)\tau_{i-1}(\vec{Q}_\parallel,\omega)\}^{-1}\tau_{i-1}(\vec{Q}_\parallel,\omega)^2, \tag{24b}$$

$$\tilde{\tau}_i(\vec{Q}_\parallel,\omega)=\{1-\tau_{i-1}(\vec{Q}_\parallel,\omega)\tilde{\tau}_{i-1}(\vec{Q}_\parallel,\omega) - \tilde{\tau}_{i-1}(\vec{Q}_\parallel,\omega)\tau_{i-1}(\vec{Q}_\parallel,\omega)\}^{-1}\tilde{\tau}_{i-1}(\vec{Q}_\parallel,\omega)^2. \tag{24c}$$

A special case of Eq. (22a) can be written as follows:

$$\mathbf{D}^R_{1,0}(\vec{Q}_\parallel,\omega)=\tau_0(\vec{Q}_\parallel,\omega)\mathbf{D}^R_{0,0}(\vec{Q}_\parallel,\omega)+\tilde{\tau}_0(\vec{Q}_\parallel,\omega)\mathbf{D}^R_{2,0}(\vec{Q}_\parallel,\omega). \tag{25}$$

If we apply Eq. (24a) successively to every $\mathbf{D}^R_{2^i,0}(\vec{Q}_\parallel,\omega)$ which appears on the right-hand side of Eq. (25), the equation is rewritten as follows:

$$\mathbf{D}^R_{1,0}(\vec{Q}_\parallel,\omega)=\tilde{\mathbf{T}}_{\rm ph}(\vec{Q}_\parallel,\omega)\mathbf{D}^R_{0,0}(\vec{Q}_\parallel,\omega) + \tilde{\tau}_0(\vec{Q}_\parallel,\omega)\tilde{\tau}_1(\vec{Q}_\parallel,\omega)\cdots\tilde{\tau}_n(\vec{Q}_\parallel,\omega)\mathbf{D}^R_{2^{n+1},0}(\vec{Q}_\parallel,\omega), \tag{26a}$$

$$\tilde{\mathbf{T}}_{\rm ph}=\tilde{\tau}_0(\vec{Q}_\parallel,\omega)+\tilde{\tau}_0(\vec{Q}_\parallel,\omega)\tilde{\tau}_1(\vec{Q}_\parallel,\omega)+\cdots + \tilde{\tau}_0(\vec{Q}_\parallel,\omega)\tilde{\tau}_1(\vec{Q}_\parallel,\omega)\cdots\tilde{\tau}_n(\vec{Q}_\parallel,\omega). \tag{26b}$$

Since $\mathbf{D}^R_{2^{n+1},0}(\vec{Q}_\parallel,\omega)\simeq\mathbf{0}$, the following approximate relation is satisfied:

$$\mathbf{D}^R_{1,0}(\vec{Q}_\parallel,\omega)\simeq\tilde{\mathbf{T}}_{\rm ph}(\vec{Q}_\parallel,\omega)\mathbf{D}^R_{0,0}(\vec{Q}_\parallel,\omega). \tag{26c}$$

Equation (21) includes the following relation:

$$\{\omega_+^2\mathbf{I}-\mathbf{K}_0(\vec{Q}_\parallel)\}\mathbf{D}^R_{0,0}(\vec{Q}_\parallel,\omega)-\mathbf{K}_+\mathbf{D}^R_{1,0}(\vec{Q}_\parallel,\omega)=\frac{\hbar}{2\pi}\mathbf{I}, \tag{27}$$

Using Eqs. (26c) and (27), we obtain the following compact expression of the retarded surface phonon Green's function of the electrode as follows:[60]

$$\mathbf{D}^R_{0,0}(\vec{Q}_\parallel,\omega)=\frac{\hbar}{2\pi}\{\omega_+^2\mathbf{I}-\mathbf{K}_0(\vec{Q}_\parallel)-\mathbf{K}_+(\vec{Q}_\parallel)\tilde{\mathbf{T}}_{\rm ph}(\vec{Q}_\parallel,\omega)\}^{-1}. \tag{28}$$

The advanced surface phonon Green's function of the electrode $\mathbf{D}^A_{0,0}(\vec{Q}_\parallel,\omega)$ is given by the complex conjugate of $\mathbf{D}^R_{0,0}(\vec{Q}_\parallel,\omega)$.

E. Mechanical contact self-energies

We assume that our chain conductor is aligned along the stacking axis of the electrodes, i.e., the z axis. Then, the phonon Green's function for the bridge-junction satisfies the following equation:

$$\begin{pmatrix} \omega_+^2\mathbf{I}_{3N_M\times3N_M}-\mathbf{K}_M & -\mathbf{K}_{L+} & \mathbf{0} \\ -\mathbf{K}_{L-} & \omega_+^2\mathbf{I}_{3N_C\times3N_C}-\mathbf{K}_C & -\mathbf{K}_{L+} \\ \mathbf{0} & -\mathbf{K}_{L-} & \omega_+^2\mathbf{I}_{3N_M\times3N_M}-\mathbf{K}_M \end{pmatrix}\begin{pmatrix} \bar{D}^R_{MM} & \bar{D}^R_{MC} & \bar{D}^R_{MM'} \\ \bar{D}^R_{CM} & \bar{D}^R_{CC} & \bar{D}^R_{CM'} \\ \bar{D}^R_{M'M} & \bar{D}^R_{M'C} & \bar{D}^R_{M'M'} \end{pmatrix}=\frac{\hbar}{2\pi}\mathbf{I}_{3N\times3N}, \tag{29}$$

where $\mathbf{I}_{3N\times3N}$ and $\mathbf{I}_{3N_C\times3N_C}$ are $3N\times3N$ and $3N_C\times3N_C$ unit matrices, respectively. The transversal force field is neglected in $\mathbf{K}_{L\pm}$ and $\mathbf{K}_C$ and the matrix components of the supermatrices in Eq. (29) are given in Appendix C Equation (29) gives the following expression of the renormalized phonon Green's function of the single molecular bridge,

$$\bar{\mathbf{D}}^R_{CC}(\omega)=\frac{\hbar}{2\pi}\left\{\omega_+^2\mathbf{I}_{3N_C\times3N_C}-\mathbf{K}_C-\sum_{L_p\neq L_q}^{L+,L-}\mathbf{K}_{L_p}(\omega_+^2\mathbf{I}_{3N_M\times3N_M}-\mathbf{K}_M)^{-1}\mathbf{K}_{L_q}\right\}^{-1}. \tag{30a}$$

As a result of the nearest-neighbor approximation, $\mathbf{K}_{L\pm}$ applies only to a single atomic site on the surface of the electrode, i.e.,

$$\mathbf{K}_{L+}(\omega_+^2\mathbf{I}_{3N_M\times3N_M}-\mathbf{K}_M)^{-1}\mathbf{K}_{L-}\simeq\frac{1}{2\pi\hbar}\mathbf{K}_{L+}\left[\int_{-\pi}^{\pi}\int_{-\pi}^{\pi}\mathbf{D}^R_{0,0}(\vec{Q}_\parallel,\omega)dQ_xdQ_y\right]\mathbf{K}_{L-}, \tag{30b}$$

Thus, the retarded phonon Green's function of the single molecular bridge given by Eq. (30a) is represented as follows:

$$\bar{\mathbf{D}}^R_{CC}(\omega)=\frac{\hbar}{2\pi}\left\{\omega_+^2\mathbf{I}_{3N_C\times3N_C}-\mathbf{K}_C-\frac{1}{2\pi\hbar}\sum_{L_p\neq L_q}^{L+,L-}\mathbf{K}_{L_p}\left[\int_{-\pi}^{\pi}\int_{-\pi}^{\pi}\mathbf{D}^R_{0,0}(\vec{Q}_\parallel,\omega)dQ_xdQ_y\right]\mathbf{K}_{L_q}\right\}^{-1}. \tag{31a}$$

Its advanced part is given by

$$\bar{\mathbf{D}}^A_{CC}(\omega)=\frac{\hbar}{2\pi}\left\{\omega_-^2\mathbf{I}_{3N_C\times3N_C}-\mathbf{K}_C-\frac{1}{2\pi\hbar}\sum_{L_p\neq L_q}^{L+,L-}\mathbf{K}_{L_p}\left[\int_{-\pi}^{\pi}\int_{-\pi}^{\pi}\mathbf{D}^A_{0,0}(\vec{Q}_\parallel,\omega)dQ_xdQ_y\right]\mathbf{K}_{L_q}\right\}^{-1}, \tag{31b}$$

where $\omega_-=\omega-i\eta$. The retarded Π^R_{contact} and the advanced Π^A_{contact} contacts self-energies between the vibrations in the conductor and the electrode phonons are therefore given by

$$\Pi^R_{\text{contact}}(\omega)=\frac{1}{2\pi\hbar}\sum_{L_p\neq L_q}^{L+,L-}\times\mathbf{K}_{L_p}\left[\int_{-\pi}^{\pi}\int_{-\pi}^{\pi}\mathbf{D}^R_{0,0}(\vec{Q}_\parallel,\omega)dQ_xdQ_y\right]\mathbf{K}_{L_q}, \tag{32a}$$

$$\Pi^A_{\text{contact}}(\omega)=\frac{1}{2\pi\hbar}\sum_{L_p\neq L_q}^{L+,L-}\times\mathbf{K}_{L_p}\left[\int_{-\pi}^{\pi}\int_{-\pi}^{\pi}\mathbf{D}^A_{0,0}(\vec{Q}_\parallel,\omega)dQ_xdQ_y\right]\mathbf{K}_{L_q}. \tag{32b}$$

Although the dimension of the Green's functions and the self-energies is written as $3N_C$, it is reduced here to N_C since the transversal force field is neglected in both $\mathbf{K}_C$, $\mathbf{K}_{L+}$, and $\mathbf{K}_{L-}$.

F. Electron Green's function

The noninteracting electronic Hamiltonian given by

$$H_e=-\sum_{\langle ij\rangle\sigma}t_{ij}(c^\dagger_{i\sigma}c_j+\text{H.c.})+\sum_{i\sigma}\varepsilon_i n_{i\sigma}, \tag{33a}$$

can be divided into the conductor part H_C, the electrodes part H_M, and the link part H_L,

$$H_C=-t\sum_{\langle ij\rangle\sigma}(c^\dagger_{i\sigma}c_j+\text{H.c.})+\varepsilon\sum_{i\sigma}n_{i\sigma}, \tag{33b}$$

$$H_M=-t_M\sum_{\langle ij\rangle\sigma}(c^\dagger_{i\sigma}c_j+\text{H.c.})+\varepsilon_M\sum_{i\sigma}n_{i\sigma}, \tag{33c}$$

$$H_L=-t_L\sum_{\langle ij\rangle\sigma}(c^\dagger_{i\sigma}c_j+\text{H.c.}), \tag{33d}$$

where the summations in H_C, H_M, and H_L are limited to the nearest-neighbor atomic pairs within the conductor, the electrodes, and the interface between the conductor and the electrodes, respectively. The link part of the Hamiltonian represents the hybridization interaction of the wave functions between the molecule and the electrodes. The retarded electron Green's function of the whole system is given by

$$\mathbf{G}^R(E)=\{(E+i\eta)\mathbf{I}-\mathbf{H}_e\}^{-1}, \tag{34a}$$

where the Hamiltonian matrix element defined on the Wannier function basis set is given by

$$(H_e)_{ij}=\begin{cases}-t_{ij} & \langle i,j\rangle\\ \varepsilon & i=j\\ 0 & \text{otherwise}\end{cases}. \tag{34b}$$

The Wannier function basis set is given by $|\chi_i\rangle\equiv c^\dagger_{i\sigma}|0\rangle$ where $|0\rangle$ is the vacuum, and the spin dependence of the single-body wave function is ignored here. Because of the semi-infiniteness of the electrodes, the dimension N of the matrices in Eq. (34a) is infinite, and the numerical calculation of the inverse matrix is not practical. Similar to the case of the phonon problem, we divide the whole single bridge-junction problem into a conductor part and two electrode parts, i.e., $N=2N_M+N_C$, where N_C is finite but N_M is infinite. Using the two-dimensional translational symmetry for the electrode and the nearest-neighbor nature of the interactions among the layers and between the molecule and the electrode, the calculation becomes free from the difficulties imposed by the infinite dimensions N_M and the calculation becomes tractable. In the following, we provide step-by-step summary of the calculation procedure regarding the electron Green's function of the molecular bridge.

G. Surface electron Green's function of electrode

Here, we describe how the surface electron Green's function is calculated.[60,61] As it has already been discussed in Sec. II D, although the electrode is assumed to be semi-infinite along the positive or the negative branch of the z axis, it is periodic on the layer defined by the x and y axes, whose translational vector is denoted by $\vec{j}_\parallel$. Then, the electronic Hamiltonian of the electrode H_M can be expressed in terms of the two-dimensional wave vector $\vec{k}_\parallel$ and the indices specifying the principal layer j_z, rather than the atomic position indices i and j,

$$H_M=-\sum_{\langle i_z,j_z\rangle}\sum_{\vec{k}_\parallel,\sigma}t_{i_z,j_z}(\vec{k}_\parallel)c^\dagger_{\vec{k}_\parallel,i_z,\sigma}c_{\vec{k}_\parallel,j_z,\sigma}+\sum_{j_z}\sum_{\vec{k}_\parallel,\sigma}\tilde{\varepsilon}(\vec{k}_\parallel)c^\dagger_{\vec{k}_\parallel,j_z,\sigma}c_{\vec{k}_\parallel,j_z,\sigma}, \tag{35a}$$

where $c_{\vec{k}_\parallel,j_z,\sigma}=1\sqrt{N_\parallel}\Sigma_{\vec{j}_\parallel}c_{\vec{j}_\parallel,j_z,\sigma}e^{i\vec{k}_\parallel\cdot\vec{R}(\vec{j}_\parallel,j_z)}$. In our case, i.e., the (001) surface which is cut out from the face center cubic structure of the electrode, $t_{i_z,j_z}(\vec{k}_\parallel)$ and $\xi_{\vec{k}_\parallel}$ are given by

$$t_{i_z,j_z}(\vec{k}_\parallel)=2t_M\left(\cos\frac{k_xa}{2}+\cos\frac{k_ya}{2}\right), \tag{35b}$$

$$\tilde{\varepsilon}(\vec{k}_\parallel)=-4t_M\cos\frac{k_xa}{2}\cos\frac{k_ya}{2}+\varepsilon_M. \tag{35c}$$

The full Hilbert space of the Hamiltonian H_M can be blocked into the subspace characterized by the quantum number $\vec{k}_\parallel$. The retarded electron Green's function, which depends on $\vec{k}_\parallel$, of the semi-infinite electrode is then given by

$$\begin{pmatrix}E_+-H_{0,0}(\vec{k}_\parallel) & -H_{0,1}(\vec{k}_\parallel) & \cdots\\ -H_{1,0}(\vec{k}_\parallel) & E_+-H_{0,0}(\vec{k}_\parallel) & -H_{0,1}(\vec{k}_\parallel)\\ \vdots & -H_{1,0}(\vec{k}_\parallel) & E_+-H_{0,0}(\vec{k}_\parallel)\\ & & \ddots\end{pmatrix}\times\begin{pmatrix}G^R_{0,0}(\vec{k}_\parallel) & G^R_{0,1}(\vec{k}_\parallel) & \cdots\\ G^R_{1,0}(\vec{k}_\parallel) & G^R_{1,1}(\vec{k}_\parallel) & \\ \vdots & & \ddots\end{pmatrix}=\mathbf{I}_{N\times N}, \tag{36}$$

where $E_+=E+i\eta$, $H_{0,0}(\vec{k}_\parallel)=\tilde{\varepsilon}(\vec{k}_\parallel)$, $H_{1,0}(\vec{k}_\parallel)=-t_{1,0}(\vec{k}_\parallel)$, and $H_{0,1}(\vec{k}_\parallel)=-t_{0,1}(\vec{k}_\parallel)$, respectively. Here, we have assumed that the transfer interaction is limited to the nearest-neighbor layers. By using recursive equations analogous to those given in Sec. II D, the retarded surface Green's function of the electrons for the electrode is obtained as follows:[60,61]

$$G^R_{0,0}(E,\vec{k}_\parallel)=[E_+-H_{0,0}(\vec{k}_\parallel)-H_{0,1}(\vec{k}_\parallel)T_e(E,\vec{k}_\parallel)]^{-1}, \tag{37a}$$

$$T_e(E,\vec{k}_\parallel)=t_0+\tilde{t}_0t_1+\tilde{t}_0\tilde{t}_1t_2+\cdots+\tilde{t}_0\tilde{t}_1\cdots\tilde{t}_{n-1}t_n, \tag{37b}$$

where

$$t_0=[E_+-H_{0,0}(\vec{k}_\parallel)]^{-1}H_{1,0}(\vec{k}_\parallel), \tag{37c}$$

$$\tilde{t}_0=[E_+-H_{0,0}(\vec{k}_\parallel)]^{-1}H_{0,1}(\vec{k}_\parallel), \tag{37d}$$

and

$$t_i=(1-t_{i-1}\tilde{t}_{i-1}-\tilde{t}_{i-1}t_{i-1})^{-1}t^2_{i-1}, \tag{37e}$$

$$\tilde{t}_i=(1-t_{i-1}\tilde{t}_{i-1}-\tilde{t}_{i-1}t_{i-1})^{-1}\tilde{t}^2_{i-1}. \tag{37f}$$

The dependences of t_i in Eqs. (37b), (37e), and (37f) on the energy E and the momentum $\vec{k}_\parallel$ are implicit. The advanced electron surface Green's function $G^A_{0,0}(E,\vec{k}_\parallel)$ is given by the complex conjugate of $G^R_{0,0}(E,\vec{k}_\parallel)$.

H. Electronic contact self-energies

The electron Green's function for the single molecular bridge satisfies the following equation:

$$\begin{pmatrix} E_+\mathrm{I}_{N_M\times N_M}-\mathbf{H}_M & -\mathbf{H}_{L+} & \mathbf{0} \\ -\mathbf{H}_{L-} & E_+\mathrm{I}_{N_C\times N_C}-\mathbf{H}_C & -\mathbf{H}_{L+} \\ \mathbf{0} & -\mathbf{H}_{L-} & E_+\mathrm{I}_{N_M\times N_M}-\mathbf{H}_M \end{pmatrix} \times \begin{pmatrix} \mathbf{G}^R_{MM} & \mathbf{G}^R_{MC} & \mathbf{G}^R_{MM'} \\ \mathbf{G}^R_{CM} & \mathbf{G}^R_{CC} & \mathbf{G}^R_{CM'} \\ \mathbf{G}^R_{M'M} & \mathbf{G}^R_{M'C} & \mathbf{G}^R_{M'M'} \end{pmatrix} = \mathbf{I}_{N\times N}. \tag{38}$$

Then, the Green's function matrix of the molecular bridge is given by

$$\mathbf{G}^R_{CC}(E)=\left[E_+\mathrm{I}_{N_C\times N_C}-\mathbf{H}_C-\sum_{L_p\neq L_q}^{L+,L-}\mathbf{H}_{L_p}(E_+\mathrm{I}_{N_M\times N_M}-\mathbf{H}_M)^{-1}\mathbf{H}_{L_q}\right]^{-1}. \tag{39}$$

The dimension of the matrix is N_C. The Hamiltonian matrix is given by Eq. (34b), and the electronic link Hamiltonians $\mathbf{H}_{L+}$ and $\mathbf{H}_{L-}$ are given in Appendix D. As a result of the nearest-neighbor approximation in $\mathbf{H}_{L\pm}$, the following relation is satisfied:

$$\mathbf{H}_{L+}(E_+\mathrm{I}_{N_M\times N_M}-\mathbf{H}_M)^{-1}\mathbf{H}_{L-} \simeq \frac{1}{4\pi^2}\mathbf{H}_{L+}\left[\int_{-\pi}^{\pi}\int_{-\pi}^{\pi}\mathbf{G}^R_{0,0}(E,\vec{k}_\parallel)dk_xdk_y\right]\mathbf{H}_{L-}, \tag{40}$$

where $G^R_{0,0}(E,\vec{k}_\parallel)$ is the retarded surface Green's function in Eq. (37a). Then, the retarded and the advanced Green's function of the electrons for the bridge-junction are given as follows:

$$\mathbf{G}^R_{CC}(E)=\left\{E_+\mathrm{I}_{N_C\times N_C}-\mathbf{H}_C-\frac{1}{4\pi^2}\times\sum_{L_p\neq L_q}^{L+,L-}\mathbf{H}_{L_p}\left[\int_{-\pi}^{\pi}\int_{-\pi}^{\pi}\mathbf{G}^R_{0,0}(E,\vec{k}_\parallel)dk_xdk_y\right]\mathbf{H}_{L_q}\right\}^{-1}, \tag{41a}$$

$$\mathbf{G}^A_{CC}(E)=\left\{E_-\mathrm{I}_{N_C\times N_C}-\mathbf{H}_C-\frac{1}{4\pi^2}\times\sum_{L_p\neq L_q}^{L+,L-}\mathbf{H}_{L_p}\left[\int_{-\pi}^{\pi}\int_{-\pi}^{\pi}\mathbf{G}^A_{0,0}(E,\vec{k}_\parallel)dk_xdk_y\right]\mathbf{H}_{L_q}\right\}^{-1}, \tag{41b}$$

where $E_-=E-i\eta$. The retarded $\mathbf{\Sigma}^R_{\mathrm{contact}}$ and the advanced $\mathbf{\Sigma}^A_{\mathrm{contact}}$ contact self-energies due to the hybridization interaction between the conductor and the electrodes are written as

$$\mathbf{\Sigma}^R_{\mathrm{contact}}(E)=\frac{1}{4\pi^2}\sum_{L_p\neq L_q}^{L+,L-}\mathbf{H}_{L_p}\left[\int_{-\pi}^{\pi}\int_{-\pi}^{\pi}\mathbf{G}^R_{0,0}(E,\vec{k}_\parallel)dk_xdk_y\right]\mathbf{H}_{L_q}, \tag{42a}$$

$$\mathbf{\Sigma}^A_{\mathrm{contact}}(E)=\frac{1}{4\pi^2}\sum_{L_p\neq L_q}^{L+,L-}\mathbf{H}_{L_p}\left[\int_{-\pi}^{\pi}\int_{-\pi}^{\pi}\mathbf{G}^A_{0,0}(E,\vec{k}_\parallel)dk_xdk_y\right]\mathbf{H}_{L_q}, \tag{42b}$$

respectively. The dimension of both the Green's functions and the self-energies are N_C.

I. Keldysh Green's function theory for transport properties

1. Overview

In Secs. II E and II H, we derived the retarded and the advanced contact self-energy arising from the hybridization interaction and mechanical coupling between the conductor and the electrodes. In addition to these, it is necessary to derive the lesser and the greater Green's functions in the Keldysh's formalism[1,62] in order to calculate the transport properties. The lesser and the greater self-energies are calculated either by solving kinetic equations[1] or by assuming thermal equilibrium.[1,63] The latter is achieved mathematically by imposing the Kadanoff-Baym boundary condition on the imaginary time axis.[63] While the boundary condition is adopted for contact self-energies, kinetic equations are solved for the vibronic self-energies of electrons and phonons arising from the nonequilibrium coupling between

them. Electrons and phonons are allowed to be thermalized only in the electrodes and are assumed to be in a nonequilibrium state in the conductor, where the energy exchange between them is possible through the electron-phonon coupling. Thus, our theory includes the nonequilibrium phonon effect on the electronic current. Associated Green's functions, i.e., the retarded, the advanced, the lesser, and the greater Green's functions are necessary as well.

2. Electronic current and energy current

Here, we make a brief review of the calculation process of the steady-state electronic current[1] and the energy current[56,64–67] through the bridge junction. We first discuss the electronic current, where we denote the lesser electronic Green's function of the extended conductor by $G_C^<(\vec{r}_1,t_1;\vec{r}_2,t_2)$, which includes all the self-energies of the electrons, i.e., the electron-phonon (e-ph) and contact self-energies. The zeroth-order lesser electronic Green's function is given by $G_C^{(0)<}(\vec{r}_1,t_1;\vec{r}_2,t_2) \equiv i\langle \Psi^\dagger(\vec{r}_1,t_1)\Psi(\vec{r}_2,t_2)\rangle$, where $\Psi^\dagger(\Psi)$ is the field creation (annihilation) operator, $\vec{r}$ and t denote the position vector and the time variable of the electrons, respectively, where the numeric subscript is the label of the electron. The total number of electrons in the conductor is given by $n_e(t)=\frac{1}{2\pi i}\int_{\text{conductor}} G_C^<(\vec{r},t;\vec{r},0)d\vec{r}$, where the space integral is taken over the conductor region. The electronic current through the conductor is defined as $j(t) \equiv -2e\frac{d}{dt}n_e(t)$, where the factor 2 results from spins, and the constant e denotes the elementary electronic charge. If we use the equation of motion for the lesser electron Green's function, the microcanonical electronic current density $j(E) \equiv \int j(t)e^{iEt/}dt$ is then given by[1]

$$j(E) = -\frac{2e}{h}\int_{\text{conductor}} [H_{xC}G_C^<(\vec{r},\vec{r}';E) - G_C^<(\vec{r},\vec{r}';E)H_{xC}]_{\vec{r}=\vec{r}'}d\vec{r}, \tag{43}$$

where $G_C^<(\vec{r},\vec{r}';E)=\int G_C^<(\vec{r},t;\vec{r}',0)e^{iEt/\hbar}dt$, $\hbar=\frac{h}{2\pi}$, and the constant h denotes the Planck constant. The Hamiltonian of the extended conductor H_{xC} satisfies the following relation:[1]

$$(E_+ - H_{xC})G_C^R(\vec{r}_1,\vec{r}_2;E) - \int d\vec{r}_3\Sigma_C^R(\vec{r}_1,\vec{r}_3;E)G_C^R(\vec{r}_3,\vec{r}_2;E) = \delta(\vec{r}_1-\vec{r}_2), \tag{44}$$

where $G_C^R(\vec{r}_1,\vec{r}_2;E)$ is the retarded electron Green's function of the extended molecule. The electron self-energy $\Sigma_C^R(\vec{r}_1,\vec{r}_3;E)$ is given by the sum of the electronic contact self-energy and the e-ph self-energy,

$$\Sigma_C^R(\vec{r}_1,\vec{r}_3;E) = \Sigma_{\text{contact}}^R(\vec{r}_1,\vec{r}_3;E) + \Sigma_{e\text{-ph}}^R(\vec{r}_1,\vec{r}_3;E), \tag{45}$$

The latter will be derived later. The first term on the right-hand side of Eq. (45) has already been derived in Sec. II H,

$$\langle \chi_i(\vec{r}_1)|\Sigma_{\text{contact}}^R(\vec{r}_1,\vec{r}_3;E)|\chi_j(\vec{r}_3)\rangle \equiv [\mathbf{\Sigma}_{\text{contact}}^R(E)]_{ij}. \tag{46a}$$

Similarly,

$$\langle \chi_i(\vec{r}_1)|\Sigma_{\text{contact}}^A(\vec{r}_1,\vec{r}_3;E)|\chi_j(\vec{r}_3)\rangle \equiv [\mathbf{\Sigma}_{\text{contact}}^A(E)]_{ij}. \tag{46b}$$

The corresponding self-adjoint relation

$$G_C^A(\vec{r}_1,\vec{r}_2;E)(E_- - H_{xC}) - \int d\vec{r}_3 G_C^A(\vec{r}_1,\vec{r}_3;E)\Sigma_C^A(\vec{r}_3,\vec{r}_2;E) = \delta(\vec{r}_1-\vec{r}_2), \tag{47}$$

is also satisfied by H_{xC}. The Dyson equations, i.e., Eqs. (44) and (47), the steady-state equations[1]

$$G_C^<(\vec{r},\vec{r}';E) = \int\int G_C^R(\vec{r},\vec{r}_1;E)\Sigma_C^<(\vec{r}_1,\vec{r}_2;E)G_C^A(\vec{r}_2,\vec{r}';E)d\vec{r}_1d\vec{r}_2, \tag{48a}$$

$$G_C^>(\vec{r},\vec{r}';E) = \int\int G_C^R(\vec{r},\vec{r}_1;E)\Sigma_C^>(\vec{r}_1,\vec{r}_2;E)G_C^A(\vec{r}_2,\vec{r}';E)d\vec{r}_1d\vec{r}_2, \tag{48b}$$

and the identity relation $\Sigma_C^>-\Sigma_C^<=\Sigma_C^R-\Sigma_C^A$ give the following formula of the microcanonical electronic current density:[1]

$$j(E) = \frac{2e}{h}\int_{\text{conductor}} [\Sigma_C^>(\vec{r},\vec{r}_1;E)G_C^<(\vec{r}_1,\vec{r}';E) - \Sigma_C^<(\vec{r},\vec{r}_1;E)G_C^>(\vec{r}_1,\vec{r}';E)]_{\vec{r}=\vec{r}'}d\vec{r}_1d\vec{r}. \tag{49a}$$

In terms of the Wannier function basis representation, this should be written as

$$j(E) = \frac{2e}{h}\text{Tr}[\Sigma_C^>(E)\mathbf{G}_C^<(E) - \Sigma_C^<(E)\mathbf{G}_C^>(E)], \tag{49b}$$

where $\mathbf{\Sigma}_C^<$ and $\mathbf{\Sigma}_C^>$ are the lesser and the greater self-energies given by

$$\mathbf{\Sigma}_C^<(E) = \mathbf{\Sigma}_{\text{contact}}^<(E) + \mathbf{\Sigma}_{e\text{-ph}}^<(E), \tag{50a}$$

$$\mathbf{\Sigma}_C^>(E) = \mathbf{\Sigma}_{\text{contact}}^>(E) + \mathbf{\Sigma}_{e\text{-ph}}^>(E), \tag{50b}$$

whose respective contributions from the hybridization interactions and the e-ph coupling will be derived in Secs. II I 3 and II I 4. The lesser (greater) contact self-energy $\mathbf{\Sigma}_{\text{contact}}^{<(>)}(E)$ is given in terms of its p and q contributions from the terminals $\mathbf{\Sigma}_{\text{contact}}^{<(>)}(E)=\mathbf{\Sigma}_p^{<(>)}(E)+\mathbf{\Sigma}_q^{<(>)}(E)$. The electronic current density $j(E)$ is decomposed into the total terminal current $j_{\text{curr}}(E)$ and the energy exchange current $j_{\text{exch}}(E)$, i.e., $j(E)=j_{\text{curr}}(E)+j_{\text{exch}}(E)$, where the latter is given by

$$j_{\text{exch}}(E) = \frac{2e}{h}\text{Tr}[\mathbf{\Sigma}_{e\text{-ph}}^>(E)\mathbf{G}_C^<(E) - \mathbf{\Sigma}_{e\text{-ph}}^<(E)\mathbf{G}_C^>(E)]. \tag{51a}$$

We have used the letters p and q as labels to distinguish the electrodes. The former can be further divided into its p and q components, i.e., $j_{\text{curr}}(E)=j_p(E)+j_q(E)$, where the terminal current at the $p(q)$ terminal is given by

$$j_{p(q)}(E) = \frac{2e}{h}\mathrm{Tr}[\boldsymbol{\Sigma}^{>}_{p(q)}(E)\mathbf{G}^{<}_{C}(E) - \boldsymbol{\Sigma}^{<}_{p(q)}(E)\mathbf{G}^{>}_{C}(E)]. \tag{51b}$$

Since $\int_{-\infty}^{\infty} j_{\mathrm{exch}}(E)dE=0$, the exchange current does not really flow, but the energy exchange with phonons $-\int_{-\infty}^{\infty}\frac{E}{e}\cdot j_{\mathrm{exch}}(E)dE \neq 0$ can be meaningful. We have only real electronic current for the terminal component, i.e., $I_{p(q)}=\int_{-\infty}^{\infty} j_{p(q)}(E)dE$. However, it should be noted that $I_p+I_q=0$ due to Kirchhoff's rule. Thus, we only have to look at either I_p or $I_q=-I_p$. We choose the former and call it $I_{\mathrm{total}}=I_p$ throughout this paper unless explicitly stated otherwise. We define the electronic energy balance of the conductor accompanying the electronic current by $Q_e=-\int_{-\infty}^{\infty}\frac{E}{e}\cdot j(E)dE$. Then, the balance is decomposed into the current $Q_{e,\mathrm{curr}}$ and the exchange $Q_{e,\mathrm{exch}}$ contributions, i.e., $Q_e=Q_{e,\mathrm{curr}}+Q_{e,\mathrm{exch}}$, where $Q_{e,\mathrm{curr}}=-\int_{-\infty}^{\infty}\frac{E}{e}\cdot j_{\mathrm{curr}}(E)dE$ and $Q_{e,\mathrm{exch}}=-\int_{-\infty}^{\infty}\frac{E}{e}\cdot j_{\mathrm{exch}}(E)dE$. The latter denotes the rate of power loss or gain of the electrons accompanying the electronic current resulting from the e-ph coupling, and the former is decomposed into p and q terminal contributions, i.e., $Q_{e,\mathrm{curr}}=Q_{e,p}+Q_{e,q}$, where $Q_{e,p(q)}=-\int_{-\infty}^{\infty}\frac{E}{e}\cdot j_{p(q)}(E)dE$. $Q_{e,p(q)}$ represents the electronic contribution to the $p(q)$ terminal energy current.

The energy flux density of phonon $q(E)$ in the conductor can be defined in terms of the energy-weighted Fourier transform of the time-dependent number density of phonons within the conductor, i.e., $h(t)\equiv dn_{\mathrm{ph}}(t)dt$, where $n_{\mathrm{ph}}(t)=-i\,\mathrm{Tr}[\mathbf{D}^{<}_{C}(t,0)]$,[56,64–67]

$$q(E) = h(E)E. \tag{52}$$

Here, $h(E)\equiv\frac{1}{2\pi}\int h(t)e^{iEt/\hbar}dt$. The lesser phonon Green's function matrix $\mathbf{D}^{<}_{C}(t,0)$ is defined as

$$[\mathbf{D}^{<}_{C}(t_1,t_2)]_{i\alpha,j\beta} \equiv i\langle[\xi_{i\alpha}(t_1),\xi_{j\beta}(t_2)]\rangle. \tag{53}$$

The flux density includes the phonon energy current density into the terminals and the energy influx from (outflux to) the electronic degrees of freedom and the latter gives the power gain (loss) of phonons. By using the equation of motion of the lesser phonon Green's function, we obtain the following general expression of the energy flux density of the phonon:[66,67]

$$q(E) = \frac{2\pi E}{h}\mathrm{Tr}[\mathbf{K}_C\mathbf{D}^{<}_{C}(E) - \mathbf{D}^{<}_{C}(E)\mathbf{K}_C], \tag{54}$$

where $\mathbf{D}^{<}_{C}(E)=\frac{1}{2\pi}\int\mathbf{D}^{<}_{C}(t,0)e^{iEt/\hbar}dt$. Taking into account the e-ph coupling effect on the phonon Green's function, the following Dyson equations should be satisfied:

$$\hbar^{-2}[E_+^2\mathbf{I}-\hbar^2\mathbf{K}_C]\mathbf{D}^{R}_{C}(E) - \Pi^{R}_{C}(E)\mathbf{D}^{R}_{C}(E) = \frac{1}{2\pi}\mathbf{I}, \tag{55a}$$

$$\mathbf{D}^{A}_{C}(E)[E_-^2\mathbf{I}-\hbar^2\mathbf{K}_C]\hbar^{-2} - \mathbf{D}^{A}_{C}(E)\Pi^{A}_{C}(E) = \frac{1}{2\pi}\mathbf{I}, \tag{55b}$$

where the phonon self-energy $\Pi^{R}_{C}(E)$ is given by the sum of the mechanical contact self-energy and the e-ph self-energy,

$$\Pi^{R}_{C}(E) = \Pi^{R}_{\mathrm{contact}}(E) + \frac{1}{2\pi}\sum_{\sigma}\Pi^{R}_{e\text{-ph},\sigma}(E). \tag{56}$$

It should be noted that $\mathbf{D}^{R(A)}_{C}(E)=\hbar^{-1}\mathbf{D}^{R(A)}_{C}(\omega)$, $\Pi^{R(A)}_{e\text{-ph},\sigma}(E)=\hbar\Pi^{R(A)}_{e\text{-ph},\sigma}(\omega)$, and $\Pi^{R(A)}_{\mathrm{contact}}(E)=\Pi^{R(A)}_{\mathrm{contact}}(\omega)$. The advanced self-energy is defined likewise, and the first term on the right-hand side of Eq. (56) has been derived in Sec. II E, while the latter term will be derived in Sec. II I 5. The Dyson equations, i.e., Eqs. (55a) and (55b), the steady-state equations,

$$\mathbf{D}^{<}_{C}(E) = 2\pi\mathbf{D}^{R}_{C}(E)\Pi^{<}_{C}(E)\mathbf{D}^{A}_{C}(E), \tag{57a}$$

$$\mathbf{D}^{>}_{C}(E) = 2\pi\mathbf{D}^{R}_{C}(E)\Pi^{>}_{C}(E)\mathbf{D}^{A}_{C}(E), \tag{57b}$$

and the identity relation $\Pi^{>}_{C}-\Pi^{<}_{C}=\Pi^{R}_{C}-\Pi^{A}_{C}$ give the following formula of the energy flux density of the phonon:

$$q(E) = \frac{2\pi E}{h}\mathrm{Tr}[\Pi^{<}_{C}(E)\mathbf{D}^{>}_{C}(E) - \Pi^{>}_{C}(E)\mathbf{D}^{<}_{C}(E)], \tag{57c}$$

where $\Pi^{<}_{C}$ and $\Pi^{>}_{C}$ are the lesser and the greater self-energies given by

$$\Pi^{<}_{C}(E) = \Pi^{<}_{\mathrm{contact}}(E) + \frac{1}{2\pi}\Pi^{<}_{e\text{-ph}}(E), \tag{58a}$$

$$\Pi^{>}_{C}(E) = \Pi^{>}_{\mathrm{contact}}(E) + \frac{1}{2\pi}\Pi^{>}_{e\text{-ph}}(E), \tag{58b}$$

whose contributions from the mechanical coupling and the e-ph coupling are derived in Secs. II I 3 and II I 5. The lesser (greater) contact self-energy $\Pi^{<(>)}_{\mathrm{contact}}(E)$ is given in terms of its p and q contributions from the terminals $\Pi^{<(>)}_{\mathrm{contact}}(E)=\Pi^{<(>)}_{p}(E)+\Pi^{<(>)}_{q}(E)$. The energy flux density of phonon $q(E)$ is decomposed to into the energy current $q_{curr}(E)$ and the energy exchange $q_{\mathrm{exch}}(E)$, i.e., $q(E)=q_{\mathrm{curr}}(E)+q_{\mathrm{exch}}(E)$, where the latter is given by

$$q_{\mathrm{exch}}(E) = \frac{E}{h}\sum_{\sigma}\mathrm{Tr}[\Pi^{<}_{e\text{-ph},\sigma}(E)\mathbf{D}^{>}_{C}(E) - \Pi^{>}_{e\text{-ph},\sigma}(E)\mathbf{D}^{<}_{C}(E)]. \tag{59a}$$

The former can be further divided into its p and q terminal components, i.e., $q_{\mathrm{curr}}(E)=q_p(E)+q_q(E)$, where the terminal energy current density at the p (q) terminal is given by

$$q_{p(q)}(E) = \frac{2\pi E}{h}\mathrm{Tr}[\Pi^{<}_{p(q)}(E)\mathbf{D}^{>}_{C}(E) - \Pi^{>}_{p(q)}(E)\mathbf{D}^{<}_{C}(E)]. \tag{59b}$$

Parallel to the electron case, we define the phonon energy balance of the conductor accompanying the phonon number current as $Q_{\mathrm{ph}}=\int_{-\infty}^{\infty}q(E)dE$. Then, the balance is decomposed into two contributions, i.e., $Q_{\mathrm{ph}}=Q_{\mathrm{ph,curr}}+Q_{\mathrm{ph,exch}}$, where $Q_{\mathrm{ph,curr}}=\int_{-\infty}^{\infty}q_{\mathrm{curr}}(E)dE$ and $Q_{\mathrm{ph,exch}}=\int_{-\infty}^{\infty}q_{\mathrm{exch}}(E)dE$. The latter represents the rate of power loss or gain of the phonons to or from the electronic degrees of freedom, and the former is divided into p and q terminal contributions, i.e., $Q_{\mathrm{ph,curr}}=Q_{\mathrm{ph},p}+Q_{\mathrm{ph},q}$, where $Q_{\mathrm{ph},p(q)}=\int_{-\infty}^{\infty}q_{p(q)}(E)dE$. $Q_{\mathrm{ph},p(q)}$ represents the phonon contribution to the $p(q)$ terminal energy

current. The rate of power loss or gain and the energy current are rigorously balanced. The energy dissipation of our vibronic system is inhibited in the conductor but is allowed in the thermalized electrodes. Within the Born and bubble approximations under the steady-state condition, $Q_{e,\mathrm{exch}}+Q_{\mathrm{ph,exch}}\simeq 0$, which will be discussed in Appendix E. Then, $Q_{e,\mathrm{curr}}+Q_{\mathrm{ph,curr}}=\Sigma_p(Q_{e,p}+Q_{\mathrm{ph},p})\simeq 0$ under the same approximation. If we define $Q_p=Q_{e,p}+Q_{\mathrm{ph},p}$, then $Q_p+Q_q\simeq 0$ approximately, and the $p(q)$ terminal energy current $Q_{p(q)}$ satisfies Kirchhoff's rule. These are also discussed in Appendix E, too. $Q_{e,p(q)}$ and $Q_{\mathrm{ph},p(q)}$ include the inelastic-scattering effects through $\mathbf{G}_C^{<(>)}(E)$ and $\mathbf{D}_C^{<(>)}(E)$ of $j_{p(q)}(E)$ and $q_{p(q)}(E)$ given by Eqs. (51b) and (59b). This and the nonequilibrium effects are the origin of our vibronic energy current. Details will be discussed in Sec. III A 4.

3. Lesser and greater contact self-energies at thermal electrodes

We assume that thermal equilibrium is achieved at the two electrodes. Then the Kadanoff-Baym boundary condition[63] can be imposed on the time variable of the electron contact self-energy $\mathbf{\Sigma}^{<}_{\mathrm{contact}}(t_1,t_2)\equiv\mathbf{\Sigma}^{<}_{p}(t_1,t_2)+\mathbf{\Sigma}^{<}_{q}(t_1,t_2)$ as follows:

$$\mathbf{\Sigma}^{<}_{p(q)}(t_1=0,t_2)=-e^{\beta_{p(q)}\mu_{p(q)}}\mathbf{\Sigma}^{>}_{p(q)}(t_1=-i\beta_{p(q)},t_2), \quad (60)$$

where $\mu_{p(q)}$ is the chemical potential of the electrode $p(q)$, and $\beta_{p(q)}=1/k_BT_{p(q)}$ is the inverse of the local temperature in the electrode $T_{p(q)}$ multiplied by the Boltzman constant k_B. The chemical potential $\mu_{p(q)}$ is determined by the voltage V in terms of $\mu_{p(q)}=E_F+\zeta_{p(q)}\mathrm{eV}$, where E_F is the Fermi level of the electrodes, and $\zeta_{p(q)}$ represents the voltage division factors which satisfy $\zeta_q-\zeta_p=1$, i.e., $\mu_q-\mu_p=eV$. We set $E_F=0$ and $\zeta_q=0.5$ throughout this paper. After performing the Fourier transform of the time variable, we use the identity relation $\mathbf{\Sigma}^{>}_{p(q)}-\mathbf{\Sigma}^{<}_{p(q)}=\mathbf{\Sigma}^{R}_{p(q)}-\mathbf{\Sigma}^{A}_{p(q)}$. Then, we obtain the following expression for the lesser and greater self-energies of the electrons at the thermalized electrodes:

$$-i\mathbf{\Sigma}^{<}_{p(q)}(E)=if_{p(q)}(E)[\mathbf{\Sigma}^{R}_{p(q)}(E)-\mathbf{\Sigma}^{A}_{p(q)}(E)], \quad (61a)$$

$$i\mathbf{\Sigma}^{>}_{p(q)}(E)=i[1-f_{p(q)}(E)][\mathbf{\Sigma}^{R}_{p(q)}(E)-\mathbf{\Sigma}^{A}_{p(q)}(E)], \quad (61b)$$

where $f_{p(q)}(E)=1[e^{\beta_{p(q)}(E-\mu_{p(q)})}+1]$ is the Fermi-Dirac distribution function for electrons at electrode $p(q)$. Likewise, the following boundary condition can be imposed on the time variable of the mechanical contact self-energy $\Pi^{<}_{\mathrm{contact}}(t_1,t_2)\equiv\Pi^{<}_{p}(t_1,t_2)+\Pi^{<}_{q}(t_1,t_2)$,

$$\Pi^{<}_{p(q)}(t_1=0,t_2)=\Pi^{>}_{p(q)}(t_1=-i\beta_{p(q)},t_2). \quad (62)$$

In contrast to the electron case, there are some differences in the sign and the chemical potential.[63] In the phonon case, the chemical potential is always zero. After performing the Fourier transform of the time, we use the identity relation $\Pi^{>}_{p(q)}-\Pi^{<}_{p(q)}=\Pi^{R}_{p(q)}-\Pi^{A}_{p(q)}$. Then, we obtain the following expression for the lesser and greater self-energies of the phonons at the thermalized electrodes:

$$-i\Pi^{<}_{p(q)}(E)=-ib_{p(q)}(E)[\Pi^{R}_{p(q)}(E)-\Pi^{A}_{p(q)}(E)], \quad (63a)$$

$$i\Pi^{>}_{p(q)}(E)=i[1+b_{p(q)}(E)][\Pi^{R}_{p(q)}(E)-\Pi^{A}_{p(q)}(E)], \quad (63b)$$

where $b_{p(q)}(E)=1/[e^{\beta_{p(q)}E}-1]$ is the Bose distribution function for phonons at electrode $p(q)$.

4. e-ph self-energies of electrons

Our perturbation Hamiltonian with respect to the electron-phonon coupling is given by

$$H_{e\text{-ph}}=\sum_{i,\sigma}\lambda t(u_{i+1z}-u_{iz})(c^{\dagger}_{i+1\sigma}c_{i\sigma}+c^{\dagger}_{i\sigma}c_{i+1\sigma}), \quad (64)$$

which was taken from Eq. (1). Here, we will derive the lesser, the greater, the retarded, and the advanced components of the self-energy corresponding to this e-ph perturbation Hamiltonian. The derivation is most clearly performed if we first derive the chronological (time-ordered) component of the self-energy, after which we adopt Langreth's formula[68] to transform the chronological self-energy to that of the lesser, the greater, the retarded, and the advanced components. The procedure is very simple, clear, and standard, and it has been frequently used in the literature.

We calculate e-ph Feynman diagrams in coordinate space but not in momentum space. Although we also do not use collective coordinates, such as normal coordinates, we must use real-space coordinates. This is due to the fact that the phonon Green's function of our bridge-junction system is obtained within the real-space formalism due to the absence of symmetry and prior information about the collective mode across the interface. The evaluation of Feynman diagrams of the e-ph coupling in real coordinate space is not standard and needs special care.[62,69,70] The perturbation Hamiltonian is off-diagonal in the atomic site index, unlike the diagonal form in the momentum space and the normal coordinate representations. This introduces certain complications into the calculation of the Feynman diagrams in real coordinate space. In the ground-state formalism, the nonvanishing contributions to the second-order chronological electron self-energy result from the contractions linked to electron external lines.[62,69,70] The chronological e-ph self-energy of electrons $\Sigma^{t}_{e\text{-ph}}(i,t_1;j,t_2)$ thus obtained is summarized in Appendix F. By using Langreth's formula,[68] we obtain the following lesser and greater self-energies:

$$[\Sigma^{<(>)}_{e\text{-ph}}(E)]_{i,j}=i2\pi\lambda^2t_L^2\sum_{\delta_1,\delta_2,\delta_3,\delta_4}\mathrm{sgn}_{\delta_1,\delta_2,\delta_3,\delta_4}\times\sum_{\sigma}\int_{-\infty}^{\infty}[G^{<(>)}_{\sigma}(E-\Lambda)]_{i+\delta_1,j+\delta_2}\times[\tilde{D}^{<(>)}(\Lambda)]_{i+\delta_3,j+\delta_4}d\Lambda, \quad (65)$$

where sgn and the sum over the displacements $\delta_1,\delta_2,\delta_3,\delta_4$ represent the signed sum in the expression of $\Sigma^{t}_{e\text{-ph}}(i,t_1;j,t_2)$ given in Appendix F.

The lesser, greater, and chronological components of the electron, as well as the phonon Green's functions $[G(E)]_{i,j}$ and $[D(\Lambda)]_{i,j}$, where the superscript specifying the compo-

nent is omitted, are classified into $\mathbf{G}_C$, $\mathbf{G}_{MM}$, $\mathbf{G}_{MC}$, and $\mathbf{G}_{CM}$ or $\mathbf{D}_C$, $\mathbf{D}_{MM}$, $\mathbf{D}_{MC}$, and $\mathbf{D}_{CM}$ depending on the region to which the indices i and j are assigned. From Eqs. (5) and (18), it is easy to notice that $\tilde{D}_{ij}(\Lambda)=(1\sqrt{M_iM_j})D_{ij}(\Lambda)$. The rule of the classification follows that used in Eqs. (29) and (38). Here, however, we used notations $\mathbf{G}_C$ and $\mathbf{D}_C$ rather than $\mathbf{G}_{CC}$ and $\bar{\mathbf{D}}_{CC}$, which are given in Eqs. (31a), (31b), (41a), and (41b), in order to emphasize that the electron-phonon self-energy effects are involved in addition to the contact self-energies as expressed in Eqs. (45) and (56). Equation (65) includes contributions from the Green's function defined between the conductor and the electrodes, i.e., $\mathbf{G}_{MC}^{<(>)}$, $\mathbf{G}_{CM}^{<(>)}$ and $\mathbf{D}_{MC}^{<(>)}$, $\mathbf{D}_{CM}^{<(>)}$. These Green's functions are given in terms of those in the electrodes and the conductors as follows:

$$\mathbf{G}_{MC}^{<(>)}(E)=\mathbf{G}_{MM}^{<(>)}(E)\mathbf{H}_{L-}\mathbf{G}_{C}^{<(>)}(E), \tag{66a}$$

$$\mathbf{G}_{CM}^{<(>)}(E)=\mathbf{G}_{C}^{<(>)}(E)\mathbf{H}_{L+}\mathbf{G}_{MM}^{<(>)}(E), \tag{66b}$$

$$\mathbf{D}_{MC}^{<(>)}(E)=\mathbf{D}_{MM}^{<(>)}(E)\mathbf{K}_{L-}\mathbf{D}_{C}^{<(>)}(E), \tag{66c}$$

$$\mathbf{D}_{CM}^{<(>)}(E)=\mathbf{D}_{C}^{<(>)}(E)\mathbf{K}_{L+}\mathbf{D}_{MM}^{<(>)}(E), \tag{66d}$$

where

$$-i\mathbf{G}_{MM}^{<}(E)=if_M(E)\{\mathbf{G}_{MM}^{R}(E)-\mathbf{G}_{MM}^{A}(E)\}, \tag{67a}$$

$$i\mathbf{G}_{MM}^{>}(E)=i\{1-f_M(E)\}\{\mathbf{G}_{MM}^{R}(E)-\mathbf{G}_{MM}^{A}(E)\}, \tag{67b}$$

$$-i\mathbf{D}_{MM}^{<}(E)=-ib_M(E)\{\mathbf{D}_{MM}^{R}(E)-\mathbf{D}_{MM}^{A}(E)\}, \tag{67c}$$

$$i\mathbf{D}_{MM}^{>}(E)=i\{1+b_M(E)\}\{\mathbf{D}_{MM}^{R}(E)-\mathbf{D}_{MM}^{A}(E)\}. \tag{67d}$$

It should be noted that both $\mathbf{G}_{MC}^{<(>)}$ and $\mathbf{G}_{CM}^{<(>)}$ depend on the link transfer integral t_L, the voltage, and the local temperature at the electrodes. The latter two dependences come from the distribution function. We have assumed thermal equilibrium within the electrodes. The dependences are unique to our real-space theory, where the nearest-neighbor interactions across the contact are taken into account within the theory for the first time. Likewise, $\mathbf{D}_{MC}^{<(>)}$ and $\mathbf{D}_{CM}^{<(>)}$ also depend on K_L. Mode couplings between the conductor and the electrodes are fully taken into account within the nearest-neighbor approximation.

5. e-ph self-energies of phonons

Parallel to the electron self-energy case, the nonvanishing contributions to the second-order chronological phonon self-energy result from the contractions linked to phonon external lines.[62,69,70] The calculation results are summarized in Appendix G. By using Langreth's formula,[68] we obtain the following lesser and greater self-energies:

$$[\Pi_{e\text{-ph},\sigma}^{<(>)}(E)]_{i,j}=i\frac{\lambda^2t_L^2}{M_C}\sum_{\delta_1,\delta_2,\delta_3,\delta_4}\mathrm{sgn}'_{\delta_1,\delta_2,\delta_3,\delta_4}\times\int_{-\infty}^{\infty}[G_\sigma^{<(>)}(E+\Lambda)]_{i+\delta_1,j+\delta_2}\times[G_\sigma^{>(<)}(\Lambda)]_{j+\delta_3,i+\delta_4}d\Lambda, \tag{68}$$

where sgn′ and the sum over the displacements $\delta_1,\delta_2,\delta_3,\delta_4$ represent the signed sum in the expression of $\Pi_{e\text{-ph},\sigma}^{t}(i,t_1;j,t_2)$ given in Appendix G. Equation (68) includes Green's function at the links which are given by Eqs. (66a)–(66d). They are dependent on the link transfer integral t_L, the voltage, and the local temperatures at the electrodes.

6. Self-consistent Born approximation

The electron and phonon Green's functions appeared in their self-energy expressions in Eqs. (65) and (68) and are expressed in terms of the self-energies in Eqs. (48a), (48b), (57a), and (57b). It is therefore necessary to solve these equations self-consistently both for electrons and phonons. This is the self-consistent Born approximation.[1,39,40] Using the self-consistent solutions, the electronic current and the energy current are calculated.

III. CALCULATIONS

In this section, the theory discussed so far is used to calculate electron transport and energy transport properties through the bridge junction in a fully consistent manner. The two transport properties are closely coupled as a result of the inelastic scatterings between electrons and phonons. Our theory guarantees that the self-consistency between them is achieved naturally. The self-consistency is highly important since phonon excitations and electron-hole excitations are closely correlated even in the steady state, and both of them exert strong influence on the transport properties.

It should be pointed out that no other published theories in the literature have taken into account the correlation satisfactorily.[53] Although the mechanical coupling between the conductor and the electrodes are important for describing the energy current through the bridge junction, it has been neglected in previous inelastic current calculations for molecules and atomic wires. In these calculations, the free boundary condition has been adopted for the vibrations of the conductor, i.e., the vibrations have been insulated thermodynamically from the bulk phonons of electrodes. They have been assumed to be in direct contact with the thermal bath, and thereby no heat transport across the vibrations of the conductor is allowed. Furthermore, these theories do not include the nonequilibrium phonon effect on the conductors. As a result of the mechanical coupling, the accurate treatment of interactions at the terminals of the conductor is important. This highlights the importance of the real-space approach, which takes into account the interactions across the contact. The structure factor of the bridge junction should not be neglected in this case. This point is oversimplified in single-level models. Moreover, although phenomenological introduction of the electron-hole excitation contribution to

the vibrational damping has been performed previously,[41–43] there have been no microscopic calculations with respect to this contribution. Our calculations are useful for investigating these problems.

In the following, we will divide our problem into two cases, i.e., (i) the isothermal case and (ii) the nonisothermal case. While the temperature gradient $\nabla \cdot T$ is set to be finite in the latter case, it is assumed to be 0 in the former case (i). The roles played by thermally nonequilibrium hot phonons will be emphasized throughout the discussions.

A. Transport properties in the isothermal condition

Here, we discuss various transport properties through the bridge junction in the isothermal condition, i.e., $\nabla \cdot T=0$. Throughout this section, we adopt $T_p=T_q=0.002/k_B=23.21$ K unless explicitly stated otherwise. The units of k_BT are eV. Before proceeding to our problem, we discuss the ballistic transmission propabilities of electrons and phonons in Secs. III A 1 and III A 2. This helps us to understand the energy-level structures of the bridge junction. Furthermore, the inelastic electronic current and the vibronic energy current will be discussed after these in Secs. III A 3 and III A 4.

The ballistic conductance of the electrons and the phonons is obtained by ignoring the electron-phonon self-energies $\Sigma_{e\text{-ph}}=0$ and $\Pi_{e\text{-ph}}=0$ for all of the Green's function components, i.e., the lesser $(>)$, the greater $(<)$, the retarded (R), and the advanced (A) components. Denoting

$$\Gamma_q(E) = i\{\mathbf{\Sigma}_q^R(E) - \mathbf{\Sigma}_q^A(E)\}, \tag{69a}$$

$$\Lambda_q(E) = i\{\Pi_q^R(E) - \Pi_q^A(E)\}, \tag{69b}$$

the lesser and the greater components of the contact self-energies given by Eqs. (61a), (61b), (63a), and (63b) can be written as follows:

$$\mathbf{\Sigma}_C^<(E) = i\sum_q f_q(E)\Gamma_q(E), \tag{70a}$$

$$\mathbf{\Sigma}_C^>(E) = -i\sum_q \{1-f_q(E)\}\Gamma_q(E), \tag{70b}$$

$$\Pi_C^<(E) = -i\sum_q b_q(E)\Lambda_q(E), \tag{70c}$$

$$\Pi_C^>(E) = -i\sum_q \{1+b_q(E)\}\Lambda_q(E). \tag{70d}$$

In the ballistic limit, the p terminal component of the electronic current density and the energy flux density of phonon are given by[1,66,67]

$$j_{p(0)}(E) = \frac{2e}{h}\sum_q T_e(E)\{f_q(E)-f_p(E)\}, \tag{71a}$$

$$q_{p(0)}(E) = \frac{1}{h}\sum_q E\cdot T_{ph}(E)\{b_q(E)-b_p(E)\}, \tag{71b}$$

where

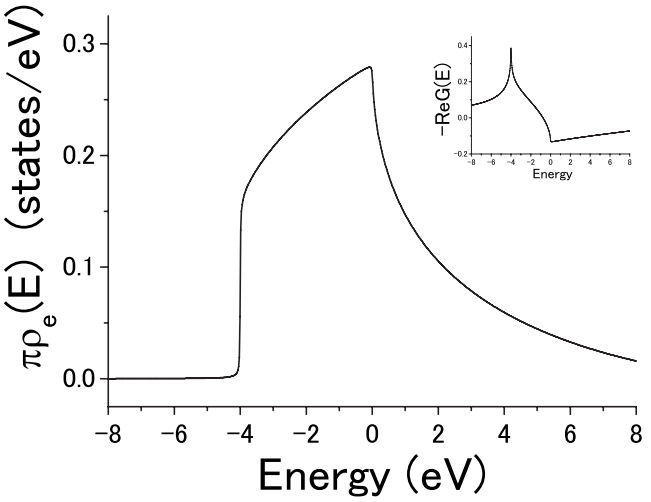

FIG. 1. The energy dependence of the electron local density of states of the electrode at the top site on the surface, i.e., $\rho_e(E)=-\frac{1}{\pi}\int_{-\pi}^{\pi}\int_{-\pi}^{\pi}[G_{0,0}^R(E,\vec{k}_\parallel)]dk_xdk_y$. The units of the energy and the local density of states are eV and states/eV, respectively. The dependence of the real part of the Green's function $-\int_{-\pi}^{\pi}\int_{-\pi}^{\pi}\mathrm{Re}[G_{0,0}^R(E,\vec{k}_\parallel)]dk_xdk_y$ on the energy is shown in the inset. The density of states in the plot is multiplied by π.

$$T_e(E) = \mathrm{Tr}[\Gamma_p(E)\mathbf{G}_{C(0)}^R(E)\Gamma_q(E)\mathbf{G}_{C(0)}^A(E)], \tag{71c}$$

$$T_{ph}(E) = 4\pi^2\,\mathrm{Tr}[\Lambda_p(E)\mathbf{D}_{C(0)}^R(E)\Lambda_q(E)\mathbf{D}_{C(0)}^A(E)], \tag{71d}$$

are their transmission probabilities. $\mathbf{G}_{C(0)}^{R(A)}(E)$ and $\mathbf{D}_{C(0)}^{R(A)}(E)$ are the retarded (advanced) electron and phonon Green's functions obtained by adopting the conditions $\mathbf{\Sigma}_{e\text{-ph}}^{R(A)}(E)=0$ and $\Pi_{e\text{-ph}}^{R(A)}(E)=0$ in Eqs. (44), (47), (55a), and (55b), respectively. These are identical to $\mathbf{G}_{CC}^{R(A)}(E)$ and $\mathbf{D}_{CC}^{R(A)}(E)$ given in Eqs. (41a), (41b), (31a), and (31b).

1. Ballistic transmission probability for electrons

First, we describe the local density of states of the electrons at the free (001) surface of the electrode cut out from the fcc lattice. The energy dependence of the local density of states of the electrons at the top site atomic position is shown in Fig. 1. The top site atomic position is located at a surface point where the terminal atom of the conductor is linked. As we place the origin of the real-space coordinate at the top site position, the local density of states is given by $-\frac{1}{\pi}\int_{-\pi}^{\pi}\int_{-\pi}^{\pi}\mathrm{Im}[G_{0,0}^R(E,\vec{k}_\parallel)]dk_xdk_y$. There is a cusp at $E_F=0$ in the local density of states, and the real part is shown in the inset of the figure. A small energy shift is expected for the conductor.

Next, we discuss the electronic structure of the whole bridge junction. The energy dependence of the ballistic transmission probabilities of electrons $T_e(E)$ are calculated for the chain conductors with $N_C=3$, 4, and 5, which are shown in Figs. 2. The trace in Eq. (71c) is taken over atomic sites. Furthermore, the calculations were made for the quasiresonant case (i), $t=-1.0$, $t_M=-1.0$, $t_L=-1.0$, $\varepsilon=0.5$, and $\varepsilon_M=0.0$, and for the tunneling case (ii), $t=-1.0$, $t_M=-1.0$,

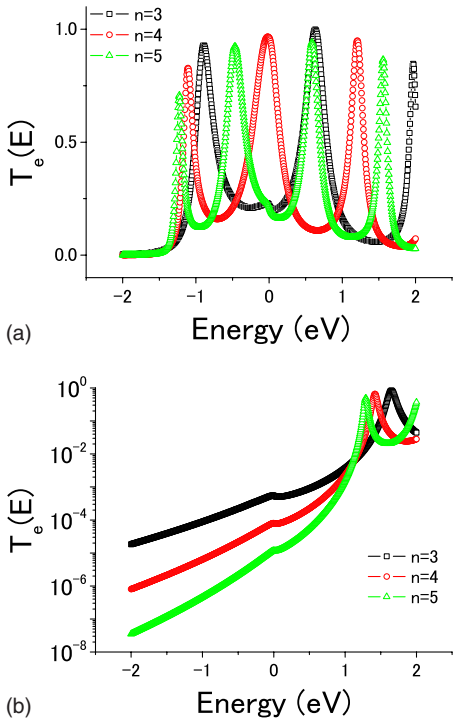

FIG. 2. (Color online) The energy dependence of the ballistic transmission probabilities $T_e(E)$ of electrons for the n site bridge junctions when $n=3$, 4, and 5. The calculations were made for the quasiresonant case (i) $t=-1.0$, $t_M=-1.0$, $t_L=-1.0$, $\varepsilon=0.5$, and $\varepsilon_M=0.0$ and the tunneling case (ii) $t=-1.0$, $t_M=-1.0$, $t_L=-1.0$, $\varepsilon=3.0$, and $\varepsilon_M=0.0$. Their results have been summarized in (a) and (b), respectively. The open squares, the open circles, and the open triangles denote the calculation results for the $n=3$, 4, and 5 site bridges, respectively.

$t_L=-1.0$, $\varepsilon=3.0$, and $\varepsilon_M=0.0$. As matter of convenience, in order to give an idea of the magnitude of the calculation results, the parameter values are given in units of eV. However, they are scalable by an arbitrary factor.

$T_e(E)$ of the even number case $N_C=4$ is the largest of all in the quasiresonant case (i) when $E=0$. In the tunneling case (ii), the transmission probability for $E=0$ correctly decreases as N_C increases. Since we adopt $E_F=0$, the conductance in the quasiresonant condition (i) is the largest when $N_C=4$, and the conductance decreases as N_C increases in the tunneling case (ii). Therefore, we will focus our attention to the $N_C=4$ case.

2. Ballistic transmission probability for phonons

Second, we discuss the transmission probability of the ballistic heat conductance of phonons $T_{\rm ph}(E)$. Before doing so, we describe the local density of states of the phonons at the top site position of the free (001) surface of the electrode cut out from the fcc lattice, i.e., $-\frac{1}{\pi}\int_{-\pi}^{\pi}\int_{-\pi}^{\pi}\mathrm{Tr}[\mathrm{Im}\{\mathbf{D}_{0,0}^{R}(\vec{Q}_{\parallel},E)\}]dQ_xdQ_y$. The trace is taken over the real-space axes, i.e., x, y, and z. The energy dependence of the local density of states is calculated and is shown in Fig. 3. Large local density of states is obtained in the energy window $E=0.025\sim0.065$.

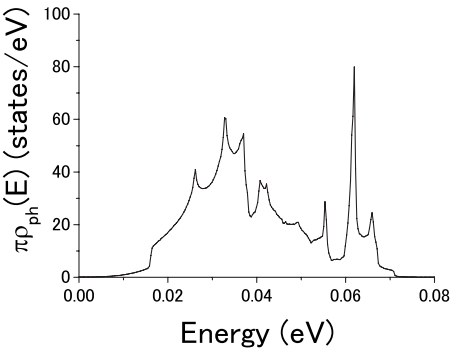

FIG. 3. The energy dependence of the phonon local density of states of the electrode at the top site on the surface, i.e., $\rho_{\rm ph}(E)=-\frac{1}{\pi}\int_{-\pi}^{\pi}\int_{-\pi}^{\pi}2|E|\mathrm{Tr}[\mathrm{Im}\{\mathbf{D}_{0,0}^{R}(\vec{Q}_{\parallel},E)\}]dQ_xdQ_y$. The units of the energy and the local density of states are eV and states/eV, respectively. The density of states in the plot is multiplied by π.

Next, we discuss the phonons in the whole bridge-junction system. It should be noted that the self-energies $\Pi_{\rm contact}^{R}$ and $\Pi_{\rm contact}^{A}$ correspond only to the z component of the surface Green's function of phonons since we have neglected the transverse components of the mechanical couplings $\mathbf{K}_{L\pm}$ given in Eqs. (C3) and (C4). The longitudinal (z) component of the local density of states of phonons (zLDOSP) at the ith site of the chain conductor given by $-\frac{1}{\pi}\mathrm{Im}[\bar{\mathbf{D}}_{CC}^{R}(E)]_{iz,iz}$ was calculated and is shown in Figs. 4. The calculations were made for a uniform case (a) $k_C=2.5$, $k_M=2.5$ and $k_L=2.5$, $M_C=M_M=1833$, a weak link case (b) $k_C=2.5$, $k_M=2.5$ and $k_L=0.5$, $M_C=M_M=1833$, and a strong link case (c) $k_C=2.5$, $k_M=2.5$ and $k_L=10.0$, $M_C=M_M=1833$. The number 1833 is an approximate value of the proton mass in units of the electron mass. The k's and M's parameters are given in the units of eV/Å^2 and $9.109\,381\,88\times10^{-31}$ kg, respectively. We describe the calculation results of the $N_C=4$ case below.

The zLDOSP for the three cases at $i=1$th, $i=2$th, $i=3$th, and $i=4$th sites are shown in Fig. 4. Owing to the symmetry (the two electrodes are identical), the zLDOSP at the $i=1$th and $i=2$th sites are identical with those of $i=4$th and $i=3$th sites, respectively. In the weak link case (b), whose results are summarized in Fig. 4(b), the lowest-energy peak of the zLDOSP, which is located at a small but finite-energy value, is fairly well overlapped or degenerated for $i=1$th, $i=2$th, $i=3$th, and $i=4$th sites. The overlap implies that all the magnitudes of the motions at the sites are identical, suggestive of translational motion. However, this is not free translational motion but is rather expected to be bound in the gap between the electrodes due to the finite energy of the peak position. The motion can be called "shuttle motion," which has been discussed both experimentally and theoretically in the literature.[71–74] The higher-energy peaks may come from intra-molecular vibrations of the conductor. In the weak link case (b), the coupling between the vibrations of the conductor and the bulk phonons of the electrodes is rather small.

On the other hand, the vibrational motions are strongly mixed in the uniform and the strong link cases (a) and (c). These were shown in Figs. 4(a) and 4(b). The position of the lowest peak is shifted to a higher energy value, and the de-

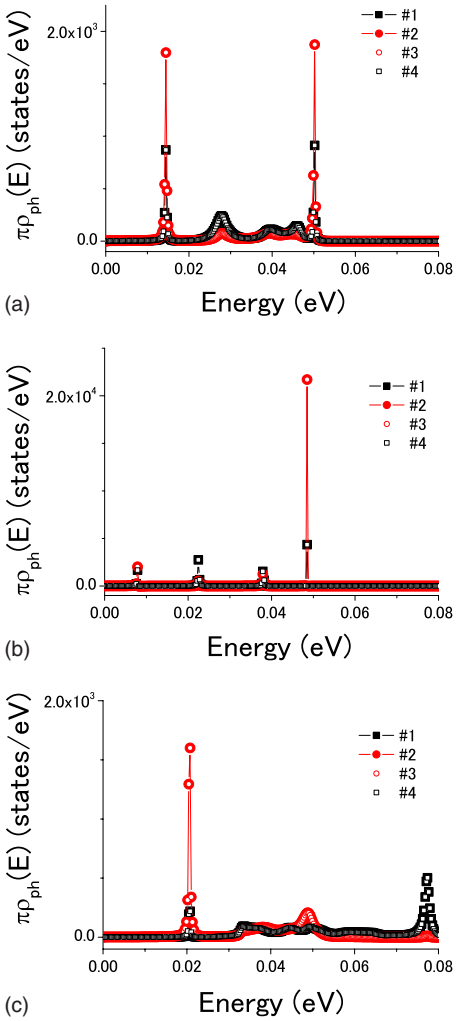

FIG. 4. (Color online) The energy dependence of the longitudinal (z) component of the phonon local densities of states of the four-site bridge at ith atomic site $\rho_{\mathrm{ph}}(E)=-\frac{1}{\pi}2|E|\mathrm{Im}[\bar{\mathbf{D}}^R_{CC}(E)]_{iz,iz}$ for a uniform case (a) $k_C=2.5$, $k_M=2.5$, $k_L=2.5$, and $M_C=M_M=1833$, a weak link case (b) $k_C=2.5$, $k_M=2.5$, $k_L=0.5$, and $M_C=M_M=1833$, and a strong link case (c) $k_C=2.5$, $k_M=2.5$, $k_L=10.0$, and $M_C=M_M=1833$ are shown in (a), (b), and (c), respectively. The units of the energy and the local density of states are eV and states/eV. The lines with solid squares, the lines with solid circles, the open circles, and the open squares denote the local densities at $i=1$, 2, 3, and 4, respectively. The density of states in the plot is multiplied by π.

generacy of the peak heights among the sites there is lifted. There exists a broad zLDOSP structure around $E=0.03\sim0.05$. The energy range agrees well with the energy window, where we obtained the large local density of states of phonons in the electrode in Fig. 3. Here too, the densities of states of the four sites are close. The appearance of the broad structure implies that vibrations in the conductor mix strongly with the bulk phonons of the electrodes. It is suggestive of a predominant contribution from the electrode around the energy range. In this energy range, vibrations in the conductor are merged into the overwhelming contribution from the bulk phonons in the electrode.

The ballistic transmission probabilities for phonon $T_{\mathrm{ph}}(E)$ given in Eq. (71d) were calculated for the three cases: (a), (b), and (c). The results are shown in Fig. 5. The probabilities remain large around the same energy range as before, i.e., $E=0.03\sim0.05$ in the cases of (a) and (c), which results from the fact that vibrational mixing between the conductor and the electrodes is very strong. The total amount of energy transported by phonons in these cases can be rather large. On the other hand, there is no such continuous structure of $T_{\mathrm{ph}}(E)$ in the weak link case of (b), where only some resonant peaks are found. The peaks are so sharp that the total amount of phonon energy transported in this case might be very small.

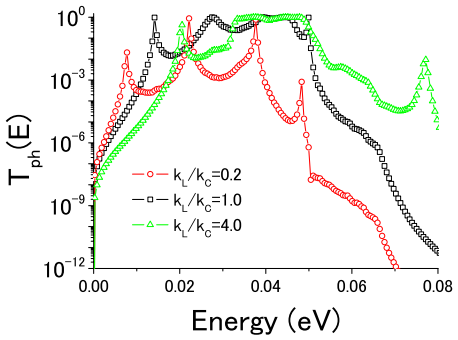

FIG. 5. (Color online) The energy dependence of the ballistic transmission probabilities of the phonon energy current $T_{\mathrm{ph}}(E)$ given in Eq. (71) for a uniform case (a) $k_C=2.5$, $k_M=2.5$, $k_L=2.5$, and $M_C=M_M=1833$, a weak link case (b) $k_C=2.5$, $k_M=2.5$, $k_L=0.5$, and $M_C=M_M=1833$, and a strong link case (c) $k_C=2.5$, $k_M=2.5$, $k_L=10.0$, and $M_C=M_M=1833$. The open squares, the open circles, and the open triangles represent the calculation results of the three cases (a), (b), and (c), respectively.

It has been found that while the intramolecular nature of the vibration in the conductor is well preserved in the weak link case, the vibration of the conductor in the uniform and the strong link cases is largely merged into the overwhelming contribution from the bulk phonons of the electrode in the energy range where large local density of states is obtained. Therefore, we have found the broad structure of zLDOSP as well as that of the transmission probability of phonons remains large in the energy range. The phonon energy transport in these cases is expected to be mostly the result of the energy range.

3. Elastic and inelastic electronic currents

We have made fully self-consistent calculations of the electronic transport and the energy transport within the Born approximation discussed in Sec. II. Here, we discuss the calculation results of the elastic and the inelastic electronic current through the bridge junction, including the electron-phonon coupling effect given in Eq. (64). The total current by default indicates the p terminal current, i.e., $I_{\mathrm{total}}=\int_{-\infty}^{\infty}j_p(E)dE$. From the combinations among the conditions (i), (ii), (a), (b), and (c), we first discuss the two cases (ib) $t=-1.0$, $t_M=-1.0$, $t_L=-1.0$, $\varepsilon=0.5$, $\varepsilon_M=0.0$, $k_C=2.5$, $k_M=2.5$, $k_L=0.5$, $M_C=M_M=1833$, and $\lambda=0.1$, and (iib) $t=-1.0$, $t_M=-1.0$, $t_L=-1.0$, $\varepsilon=3.0$, $\varepsilon_M=0.0$, $k_C=2.5$, $k_M=2.5$, $k_L=0.5$, $M_C=M_M=1833$, and $\lambda=0.1$. The electron-phonon coupling constant is fixed to $\lambda=0.1$ throughout this paper,

and the units of λ are 1/Å. The dependence on the bias voltage V of the second derivatives of the elastic and inelastic currents d^2I_Δ/dV^2 and $d^2I_{\text{inelastic}}/dV^2$, where[28]

$$I_{\text{elastic}} = \frac{2e}{h}\sum_q \int_{-\infty}^{\infty} \text{Tr}[\boldsymbol{\Sigma}_p^{>}(E)\mathbf{G}_q^{<}(E) - \boldsymbol{\Sigma}_p^{<}(E)\mathbf{G}_q^{>}(E)]dE, \tag{72a}$$

$$I_{\text{inelastic}} = \frac{2e}{h}\int_{-\infty}^{\infty} \text{Tr}[\boldsymbol{\Sigma}_p^{>}(E)\mathbf{G}_{e-ph}^{<}(E) - \boldsymbol{\Sigma}_p^{<}(E)\mathbf{G}_{e-ph}^{>}(E)]dE, \tag{72b}$$

was calculated for $N_C=4$. Here, $I_\Delta = I_{\text{elastic}} - I_{\text{ballistic}}$, $\mathbf{G}_q^{<(>)}(E) = \mathbf{G}_C^R(E)\boldsymbol{\Sigma}_q^{<(>)}(E)\mathbf{G}_C^A(E)$, and $\mathbf{G}_{e\text{-ph}}^{<(>)}(E) = \mathbf{G}_C^R(E)\boldsymbol{\Sigma}_{e\text{-ph}}^{<(>)}(E)\mathbf{G}_C^A(E)$. In addition, $I_{\text{ballistic}} = \int_{-\infty}^{\infty} j_{p(0)}(E)dE$, where $j_{p(0)}(E)$ is given in Eq. (71a). The total current is given by the sum of the two current components: $I_{\text{total}} = I_{\text{elastic}} + I_{\text{inelastic}}$. Equations (72a) and (72b), derived from Eq. (51b), are equivalent to the following familiar forms:[1]

$$I_{\text{elastic}} = \frac{2e}{h}\sum_q \int_{-\infty}^{\infty} \text{Tr}[\Gamma_p(E)\mathbf{G}_C^R(E)\Gamma_q(E)\mathbf{G}_C^A(E)] \times \{f_q(E) - f_p(E)\}dE, \tag{73a}$$

$$I_{\text{inelastic}} = i\frac{2e}{h}\int_{-\infty}^{\infty} \text{Tr}[\boldsymbol{\Sigma}_p^{<}(E)\mathbf{G}_C^R(E)\Gamma_{e-ph}(E)\mathbf{G}_C^A(E) - \Gamma_p(E)\mathbf{G}_C^R(E)\boldsymbol{\Sigma}_{e\text{-ph}}^{<}(E)\mathbf{G}_C^A(E)]dE, \tag{73b}$$

where $\Gamma_{e\text{-ph}}(E) = i[\boldsymbol{\Sigma}_{e\text{-ph}}^R(E) - \boldsymbol{\Sigma}_{e\text{-ph}}^A(E)]$.

In the case (ib), we observed a large electron-phonon coupling effect in both the elastic and the inelastic channels, which is shown in Fig. 6(a). This is due to the fact that one of the electronic energy levels of the conductor in this case is quasiresonant with E_F. This is clearly understood from Fig. 2, which indicates that the ballistic transmission probability is largest around E_F. In the elastic channel, a peak of d^2I_Δ/dV^2 is located at a voltage value corresponding to a negative phonon energy, i.e., $V=-0.05$, and a dip is located at a positive phonon energy, i.e., $V=0.05$. In contrast to the elastic channel, a peak and a dip of $d^2I_{\text{inelastic}}/dV^2$ are located at voltage value corresponding to positive and negative phonon energies, respectively. The bias voltage dependence of $d^2I_{\text{inelastic}}/dV^2$ is reversed compared with that of d^2I_Δ/dV^2.[49,50] While the latter indicates that the resistance increases as phonons become excited, the former implies that a decrease in the resistance accompanies phonon excitation. In the inelastic channel, a curious and counterintuitive phenomenon appears, where the elastic response is larger in magnitude than the inelastic one in the quasiresonant case (ib). We therefore observe a peak and a dip of d^2I_{total}/dV^2 at negative and positive phonon energies, respectively. Such behavior can be expected in atomic wires.

If we take a close look at Fig. 6(a), it is not be difficult to notice that the offsets appear in both the d^2I_Δ/dV^2 and $d^2I_{\text{inelastic}}/dV^2$ plots when $|V|$ is larger than that of the peak or the dip position, i.e., neither of the second derivatives falls off to zero immediately. The offset of d^2I_Δ/dV^2 is negative at the positive branch of V and positive at the negative branch. However, $d^2I_{\text{inelastic}}/dV^2$ behaves quite differently, i.e., the offset in this case is positive (negative) at the positive (negative) branch. In the two cases of d^2I_Δ/dV^2 and $d^2I_{\text{inelastic}}/dV^2$ of (ib), the offset takes the same sign as that of a nearby dip or peak. Due to the dominance of the elastic response over the inelastic response in the quasiresonant case (ib), the offset of $d^2I_{\text{total}(\Delta)}/dV^2$, where $I_{\text{total}(\Delta)} = I_{\text{total}} - I_{\text{ballistic}} = I_\Delta + I_{\text{inelastic}}$, is negative and positive at the positive and the negative branches of V, respectively. This is shown in the

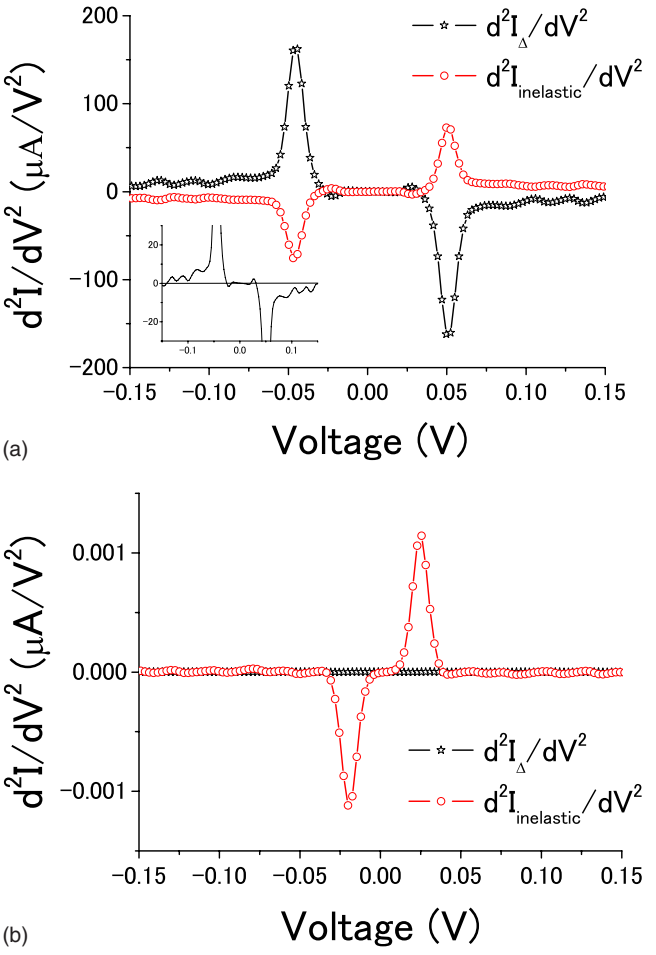

FIG. 6. (Color online) The elastic and the inelastic contributions to the shape of the plot representing the voltage dependence of d^2I/dV^2. $I_\Delta = I_{\text{elastic}} - I_{\text{ballistic}}$. $I_{\text{ballistic}} = \int j_{p(0)}(E)dE$, where $j_{p(0)}(E)$ is given in Eq. (71). I_{elastic} and $I_{\text{inelastic}}$ are given in Eqs. (72a) and (72b), respectively. The total electronic current is given by $I_{\text{total}} = I_{\text{elastic}} + I_{\text{inelastic}}$. The calculation results for the two cases (ib) $t=-1.0$, $t_M=-1.0$, $t_L=-1.0$, $\varepsilon=0.5$, $\varepsilon_M=0.0$, $k_C=2.5$, $k_M=2.5$, $k_L=0.5$, $M_C=M_M=1833$, and $\lambda=0.1$ and (iib) $t=-1.0$, $t_M=-1.0$, $t_L=-1.0$, $\varepsilon=3.0$, $\varepsilon_M=0.0$, $k_C=2.5$, $k_M=2.5$, $k_L=0.5$, $M_C=M_M=1833$, and $\lambda=0.1$ are summarized in the plots (a) and (b), respectively. The open stars and the open circles denote the calculation results of d^2I_Δ/dV^2 and $d^2I_{\text{inelastic}}/dV^2$. In the inset of (a), $d^2I_{\text{total}(\Delta)}/dV^2$, where $I_{\text{total},(\Delta)} = I_{\text{total}} - I_{\text{ballistic}}$ is given in the same voltage range as that of (a) and (b), and the straight line in the inset denotes the horizontal axis. The units of the voltage and d^2I/dV^2 are V and $\mu\text{A}/V^2$, respectively. $k_BT=0.002(T=23.21\ \text{K})$ in all cases.

inset of Fig. 6(a). The offset decreases with an additional oscillation as $|V|$ increases. Apart from the oscillative factor, the suppression of the total electronic current $\delta|I_{\text{total}}|$ due to the electron-phonon coupling beyond the threshold voltage (the phonon energy) can be roughly approximated as $\delta|I_{\text{total}}| \sim -|V|^{\theta}$, where $1 \leq \theta \leq 2$. It is well known that we have no offsets in the calculation results of d^2I/dV^2 obtained when $\Pi(E)=0$.[39,40] Therefore, the offset might be closely related with vibrational damping.

The calculation results for the case (iib) are summarized in Fig. 6(b). We first noticed that the magnitudes of the peak and the dip are exponentially reduced compared with those of the case (ib) given in Fig. 6(a) in both the elastic and the inelastic channels, where the reduction factor was about 1×10^{-5} for the inelastic channel, while the ratio for the elastic channel is much smaller than that for the inelastic one. Electrons in the conductor are kept apart from those in the electrodes due to the large electronic energy gap $\Delta E=|\varepsilon-E_F|$. Although the elastic response is negligible in the tunneling case (iib), the inelastic response remains finite, in sharp contrast to the case (ib), where the elastic channel is dominant. The similar bias voltage dependence as that in the case (ib) was found for $d^2I_{\text{inelastic}}/dV^2$. We therefore observe a small peak and a small dip of d^2I_{total}/dV^2 at positive and negative of the phonon energies, i.e., $V=\pm 0.03$, respectively. Such behavior can be expected in molecular wires. It should be noted that the absolute value of the peak position here is shifted to $|V|=0.03$ as compared with that obtained in the quasiresonant case (ia), i.e., $|V|=0.05$. The phonon mode which has the largest influence on the electron transport is different in the quasiresonant case and the tunneling case, irrespective of the uniqueness of the phonons and the electron-phonon coupling, and dependent on the electron density in the conductor. The offset was not observed in this case. The enhancement of the total electronic current $\delta|I_{\text{total}}|$ due to the electron-phonon coupling beyond the threshold voltage is therefore proportional to $\delta|I_{\text{total}}| \sim |V|$.

The k_L dependence of $d^2I_{\text{total}(\Delta)}/dV^2$ is calculated for the quasiresonant (i) and the tunneling (ii) cases. k_L is changed in the three cases: (a), (b), and (c). The calculation results obtained by using the two electronic parameter sets (i) and (ii) are summarized in Figs. 7(a) and 7(b), respectively. Small shifts of the peak positions were observed as k_L/k_C was changed to 0.2, 1.0, and 4.0 in the quasiresonant cases (i), i.e., the cases (ib) $t=-1.0$, $t_M=-1.0$, $t_L=-1.0$, $\varepsilon=0.5$, $\varepsilon_M=0.0$, $k_C=2.5$, $k_M=2.5$, $k_L=0.5$, $M_C=M_M=1833$, and $\lambda=0.1$, (ia) $t=-1.0$, $t_M=-1.0$, $t_L=-1.0$, $\varepsilon=0.5$, $\varepsilon_M=0.0$, $k_C=2.5$, $k_M=2.5$, $k_L=2.5$, $M_C=M_M=1833$, and $\lambda=0.1$, and (ic) $t=-1.0$, $t_M=-1.0$, $t_L=-1.0$, $\varepsilon=0.5$, $\varepsilon_M=0.0$, $k_C=2.5$, $k_M=2.5$, $k_L=10.0$, $M_C=M_M=1833$, and $\lambda=0.1$. Fair dependences on k_L were found for the offsets in the same cases. This suggests that the mechanical coupling between the conductor and the electrodes has a large influence on the vibrational damping in the quasiresonant condition (i). The magnitude of the offset is reduced as k_L increases. As a counterintuitive result, larger vibrational dampings favor weaker links. This suggests that the electron-hole excitation is the major path for the vibrational damping in the quasiresonant case (i), and the contribution of the resonant electron-hole excitation increases as the mechanical link

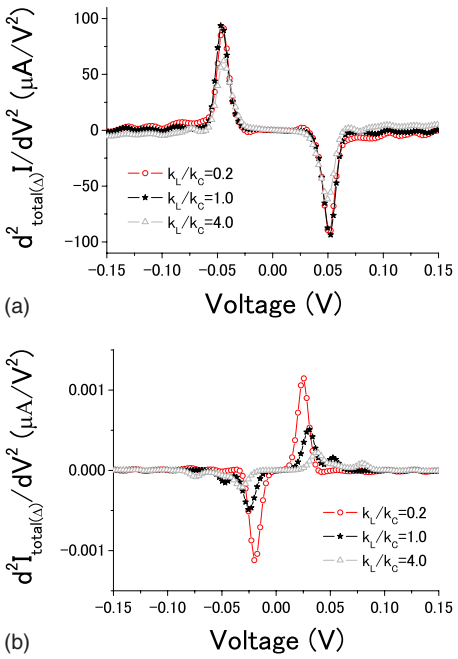

FIG. 7. (Color online) The dependence of $d^2I_{\text{total}(\Delta)}/dV^2$, where $I_{\text{total}(\Delta)}=I_{\text{total}}-I_{\text{ballistic}}$ on the link force field. The calculation results for the quasiresonant case (i) $t=-1.0$, $t_M=-1.0$, $t_L=-1.0$, $\varepsilon=0.5$, and $\varepsilon_M=0.0$ and the tunneling case (ii) $t=-1.0$, $t_M=-1.0$, $t_L=-1.0$, $\varepsilon=3.0$, and $\varepsilon_M=0.0$ are summarized in (a) and (b). The force field is changed among the three cases, i.e., a uniform case (1) $k_C=2.5$, $k_M=2.5$, $k_L=2.5$, and $M_C=M_M=1833$, a weak link case (2) $k_C=2.5$, $k_M=2.5$, $k_L=0.5$, and $M_C=M_M=1833$, and a strong link case (3) $k_C=2.5$, $k_M=2.5$, $k_L=10.0$, and $M_C=M_M=1833$. $\lambda=0.1$ for all cases studied here. The closed stars, the open circles, and the open triangles denote the calculation results of the uniform case (1), the weak link case (2), and the strong link case (3). The units of voltage and d^2I/dV^2 are V and $\mu A/V^2$, respectively. $k_BT=0.002(T=23.21\ \text{K})$ in all cases.

weakens. A change in the sign of the offset accompanies the further increase of k_L from (ia) to (ic). There are no offsets in the tunneling case (ii). The peak position is blueshifted, and its width becomes large as the link k_L becomes stronger. The blueshift and the width enhancement indicate the existence of substantial contributions of the mechanical coupling to these quantities. However, its contribution to the offset is small due to the large electronic gap $\Delta E=|\varepsilon-E_F|$. There is no contribution from the electron-hole excitation to the offset in this case. In the tunneling electron system, due to the absence of the large contribution of the electron-hole excitation, the role played by the mechanical link is more prominent than that in the quasiresonant system.

The k_L dependence of $dI_{\text{total}(\Delta)}/dV$ has been calculated for the quasiresonant cases (ia), (ib), and (ic) and the results are summarized in Fig. 8. It should be stressed that no significant electron-phonon-scattering effects were found below the phonon energy corresponding to $V=0.05$. We did not find any clear responses in low-energy phonons as far as our SSH model is concerned. There appears to be a propensity rule working for the vibronic responses of the electronic current.[38–40,47,48,50] Since the propensity rule favors higher-energy phonon modes, nearly ballistic electronic transport

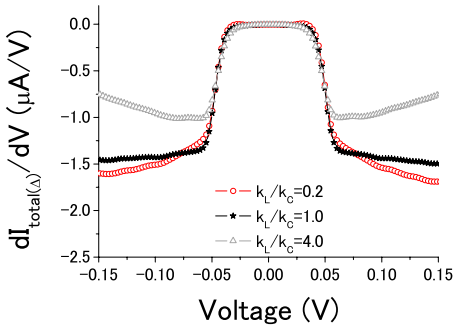

FIG. 8. (Color online) The dependence of $dI_{\text{total}(\Delta)}/dV$. $I_{\text{total}(\Delta)}=I_{\text{total}}-I_{\text{ballistic}}$ on the link force field. The calculation result for the quasiresonant case (i) $t=-1.0$, $t_M=-1.0$, $t_L=-1.0$, $\varepsilon=0.5$, and $\varepsilon_M=0.0$ is shown. The force field is different in each of the three cases, i.e., a uniform case (a) $k_C=2.5$, $k_M=2.5$, $k_L=2.5$, and $M_C=M_M=1833$, a weak link case (b) $k_C=2.5$, $k_M=2.5$, $k_L=0.5$, and $M_C=M_M=1833$, and a strong link case (c) $k_C=2.5$, $k_M=2.5$, $k_L=10.0$, and $M_C=M_M=1833$. $\lambda=0.1$ for all cases studied here. The closed stars, the open circles, and the open triangles represent the calculation results of $dI_{\text{total}(\Delta)}/dV$ of the three cases (a), (b), and (c), respectively. The units of voltage and dI/dV are V and $\mu A/V$, respectively. $k_BT=0.002(T=23.21\ \text{K})$ in all cases.

might be possible in atomic and molecular scale conductors in spite of the fact that the significant inelastic effects are expected for some of their vibrational modes. The change in the slope beyond $|V|>0.05$ in the three plots of the figure corresponds to the sign change in the offset value discussed in Fig. 7(a). The sign change is more clearly understood as the upturn of the slope accompanying the increase of k_L from (ia) to (ic) in Fig. 8. The sign change in $d^2I_{\text{total}(\Delta)}/dV^2$ very close to the peak and the dip positions is suggestive of the strong nonlinearity of the current-voltage curve.

4. Vibronic energy current

The influence of electron-phonon coupling on the energy current in the isothermal condition is discussed here. As already stated before, we adopt $T_p=T_q=0.002/k_B=23.21$ K. Considering that $Q_p+Q_q\simeq 0$, where $Q_{p(q)}=Q_{e,p(q)}+Q_{\text{ph},p(q)}$, the energy current which we need to focus on can be given as follows: $Q_p=Q_{e,p}+Q_{\text{ph},p}$, where $Q_{e,p}=-\int_{-\infty}^{\infty}\frac{E}{e}\cdot j_p(E)dE$ and $Q_{\text{ph},p}=\int_{-\infty}^{\infty}q_p(E)dE$. Both $Q_{e,p}$ and $Q_{\text{ph},p}$ are decomposed into their respective elastic and inelastic contributions, as already done in Eqs. (72a), (72b), (73a), and (73b),

$$Q_{e,p}=Q_{e,p}^{\text{elastic}}+Q_{e,p}^{\text{inelastic}}, \tag{74a}$$

$$Q_{e,p}^{\text{elastic}}=-\frac{2}{h}\sum_q\int_{-\infty}^{\infty}E\cdot\bar{T}_e(E)\{f_q(E)-f_p(E)\}dE, \tag{74b}$$

$$Q_{e,p}^{\text{inelastic}}=-i\frac{2}{h}\int_{-\infty}^{\infty}E\cdot\text{Tr}[\boldsymbol{\Sigma}_p^{<}(E)\mathbf{G}_C^R(E)\Gamma_{e\text{-ph}}(E)\mathbf{G}_C^A(E)-\Gamma_p(E)\mathbf{G}_C^R(E)\boldsymbol{\Sigma}_{e\text{-ph}}^{<}(E)\mathbf{G}_C^A(E)]dE, \tag{74c}$$

$$\bar{T}_e(E)=\text{Tr}[\Gamma_p(E)\mathbf{G}_C^R(E)\Gamma_q(E)\mathbf{G}_C^A(E)]. \tag{74d}$$

Here $\bar{T}_e(E)$ is the elastic transmission probability of electrons and is different from the ballistic transmission probability for electrons as given in Eq. (71c). The decomposition of $Q_{\text{ph},p}$ is similarly given by

$$Q_{\text{ph},p}=Q_{\text{ph},p}^{\text{elastic}}+Q_{\text{ph},p}^{\text{inelastic}}, \tag{75a}$$

$$Q_{\text{ph},p}^{\text{elastic}}=\frac{1}{h}\sum_q\int_{-\infty}^{\infty}E\cdot\bar{T}_{\text{ph}}(E)\{b_q(E)-b_p(E)\}dE, \tag{75b}$$

$$Q_{\text{ph},p}^{\text{inelastic}}=i\frac{2\pi}{h}\int_{-\infty}^{\infty}E\cdot\text{Tr}[\Lambda_p(E)\mathbf{D}_C^R(E)\Pi_{e\text{-ph}}^{<}(E)\mathbf{D}_C^A(E)-\Pi_p^{<}(E)\mathbf{D}_C^R(E)\Lambda_{e\text{-ph}}(E)\mathbf{D}_C^A(E)]dE, \tag{75c}$$

$$\bar{T}_{\text{ph}}(E)=\text{Tr}[\Lambda_p(E)\mathbf{D}_C^R(E)\Lambda_q(E)\mathbf{D}_C^A(E)]. \tag{75d}$$

Here $\bar{T}_{\text{ph}}(E)$ is the elastic transmission probability for phonons and is different from the ballistic phonon transmission probability given in Eq. (71d). Although the phonon Green's function $\mathbf{D}_C^{R(A)}(E)$ in Eq. (75d) includes the vibronic self-energy $\Pi_{e\text{-ph}}^{R(A)}(E)$ given in terms of the electron Green's function $\mathbf{D}_{C(0)}^{R(A)}(E)$ in Eq. (71d) does not include the self-energy $\Pi_{e\text{-ph}}^{R(A)}(E)$. It will be interesting to divide the energy current Q_p into its elastic and inelastic contributions, i.e., $Q_p=Q_p^{\text{elastic}}+Q_p^{\text{inelastic}}$, where $Q_p^{\text{elastic}}=Q_{e,p}^{\text{elastic}}+Q_{\text{ph},p}^{\text{elastic}}$ and $Q_p^{\text{inelastic}}=Q_{e,p}^{\text{inelastic}}+Q_{\text{ph},p}^{\text{inelastic}}$. As a result of Eqs. (74b) and (75b), $Q_{e,p}^{\text{elastic}}+Q_{e,q}^{\text{elastic}}=0$ and $Q_{\text{ph},p}^{\text{elastic}}+Q_{\text{ph},q}^{\text{elastic}}=0$, and hence, $Q_p^{\text{elastic}}+Q_q^{\text{elastic}}=0$ in our two terminal system. Following the discussions given in Appendix E, it can be said that $Q_p^{\text{inelastic}}+Q_q^{\text{inelastic}}\simeq 0$, which is the reason for writing the relation $Q_p+Q_q\simeq 0$. When the e-ph coupling constant vanishes, i.e., $\lambda\to 0$, $Q_{\text{ph},p}^{\text{elastic}}$ is reduced to the ballistic one, i.e., $Q_{\text{ph},p}^{\text{elastic}}\to\int_{-\infty}^{\infty}q_{p(0)}(E)dE$, where $q_{p(0)}(E)$ is given in Eq. (71b). If we introduce a small temperature difference ΔT across the bridge junction, i.e., $T_q=T$ and $T_p=T+\Delta T$, it is easy to find that $\frac{1}{\Delta T}Q_{\text{ph},p}^{\text{elastic}}$ is reduced to the standard formula of the phonon heat conductance found in the literature,[56,66,67] i.e., $\frac{1}{\Delta T}Q_{\text{ph},p}^{\text{elastic}}\to\frac{k_B^2T}{h}\int_{-\infty}^{\infty}T_{\text{ph}}(k_BTx)\frac{x^2}{(e^x-1)^2}dx$ in the limit of $\lambda\to 0$ and $\Delta T\to 0$. In the isothermal condition, $Q_{\text{ph},p(q)}^{\text{elastic}}=0$ due to the cancellation of the Bose factors in Eq. (75b). Since we are interested in the inelastic effects on the energy current, we will mainly focus our attention to $Q_p^{\text{inelastic}}$ in the subsequent discussion.

The energy dependence of $\bar{T}_{\text{ph}}(E)$ on the case (a), i.e., for $k_L/k_C=1.0$, is calculated for (i) the quasiresonant and (ii) the tunneling parameter sets for electrons, and they are summarized in Fig. 9. As a reference, the ballistic transmission probability $T_{\text{ph}}(E)$ of the same case (a) $k_L/k_C=1.0$ is also plotted in the same figure. The elastic phonon transmission probability $\bar{T}_{\text{ph}}(E)$ for the tunneling parameter set (iia) agrees well with the ballistic phonon transmission probability $T_{\text{ph}}(E)$. Due to the large electronic gap, $\Delta E=|\varepsilon-E_F|$, the self-energy $\Pi_{e\text{-ph}}^{R(A)}(E)$ plays a minor role in this tunneling case. On the other hand, we found a clear difference between the two transmission probabilities in the resonant case (ia). The peak

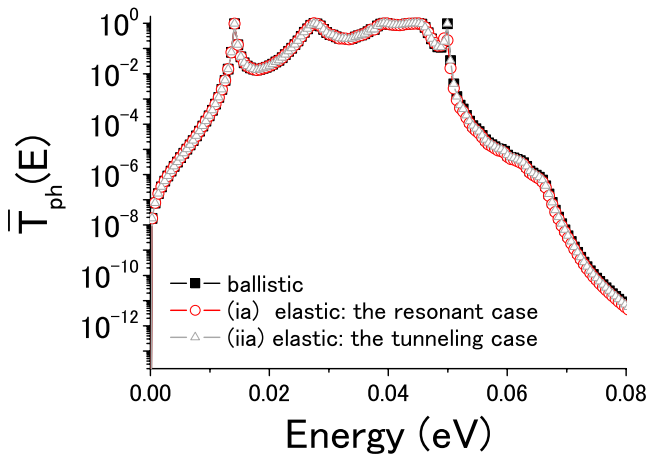

FIG. 9. (Color online) The dependence of the elastic transmission probabilities on the energy of the phonon energy current $\bar{T}_{\mathrm{ph}}(E)$ given in Eq. (74c). The calculation results for the two cases (ia) $t=-1.0$, $t_M=-1.0$, $t_L=-1.0$, $\varepsilon=0.5$, $\varepsilon_M=0.0$, $k_C=2.5$, $k_M=2.5$, $k_L=2.5$, $M_C=M_M=1833$, and $\lambda=0.5$ and (iia), $t=-1.0$, $t_M=-1.0$, $t_L=-1.0$, $\varepsilon=3.0$, $\varepsilon_M=0.0$, $k_C=2.5$, $k_M=2.5$, $k_L=2.5$, $M_C=M_M=1833$, and $\lambda=0.5$ are compared with the ballistic transmission probability. The closed squares, the open circles, and the open triangles represent the ballistic transmission probability, the elastic transmission probability calculated for the quasiresonant case (ia), and the elastic transmission probability calculated for the tunneling case (iia), respectively.

of the ballistic transmission probability $T_{\mathrm{ph}}(E)$ close to $E \simeq 0.05$ is reduced significantly in the elastic phonon transmission probability $\bar{T}_{\mathrm{ph}}(E)$ of the quasiresonant parameter set (ia). The energy coincides with the position of the dip of $d^2I_{\mathrm{total}(\Delta)}/dV^2$ calculated for the quasiresonant condition (ia) for electrons. This is indicative of the strong inelastic electron-phonon coupling effects on the phonon energy transport. This coincidence suggests that the phonon energy transport is closely correlated with the electron transport.

In order to understand the correlation more clearly, we studied the voltage dependence of the p terminal energy current $Q_p^{\mathrm{inelastic}}$ and its contributions from electron and phonon $Q_{e,p}^{\mathrm{inelastic}}$ and $Q_{\mathrm{ph},p}^{\mathrm{inelastic}}$, which are given in Eqs. (74c) and (75c), i.e., $Q_p^{\mathrm{inelastic}}=Q_{e,p}^{\mathrm{inelastic}}+Q_{\mathrm{ph},p}^{\mathrm{inelastic}}$. The calculation results obtained by using the quasiresonant parameter set (ia) are summarized in Fig. 10. The signs of $Q_{e,p}^{\mathrm{inelastic}}$ and $Q_{ph,p}^{\mathrm{inelastic}}$ are opposite. The magnitude of both $Q_{e,p}^{\mathrm{inelastic}}$ and $Q_{\mathrm{ph},p}^{\mathrm{inelastic}}$ is enhanced at the same threshold bias voltage values $V=\pm 0.05$ corresponding to the peak or the dip position of $d^2I_{\mathrm{total}(\Delta)}/dV^2$ given in Fig. 7(a), suggestive of the important role of the inelastic scatterings in the enhancement. In both cases, the enhancement is asymmetric with regard to the sign change in V; i.e., the slopes $\partial Q_{e,p}^{\mathrm{inelastic}}/\partial V$ and $\partial Q_{\mathrm{ph},p}^{\mathrm{inelastic}}/\partial V$ take different absolute values in the positive and the negative branches of V. The voltage dependences of their magnitudes are different; i.e., while the magnitude of the slope is larger in the positive branches of V than in the negative branch for $Q_{\mathrm{ph},p}^{\mathrm{inelastic}}$, it is smaller there for $Q_{e,p}^{\mathrm{inelastic}}$. As a result of the asymmetry, the difference, and the signs, the inelastic energy current $Q_p^{\mathrm{inelastic}}$, which is given by the sum of $Q_{e,p}^{\mathrm{inelastic}}$ and $Q_{ph,p}^{\mathrm{inelastic}}$, remains finite after the cancellation of the two contributions. Furthermore, due to the thresholdlike increase in $|Q_{e,p}^{\mathrm{inelastic}}|$ and $|Q_{\mathrm{ph},p}^{\mathrm{inelastic}}|$ at $V=\pm 0.05$, $Q_p^{\mathrm{inelastic}}$ is enhanced at the same voltage value. $Q_p^{\mathrm{inelastic}}$ changes its sign when $V \to -V$. The inelastic energy balance, i.e., the sum of the two inelastic energy currents at the two terminals remains close to zero, i.e., $Q_p^{\mathrm{inelastic}}+Q_q^{\mathrm{inelastic}} \simeq 0$. The small deviation from the expected relation $Q_p^{\mathrm{inelastic}}+Q_q^{\mathrm{inelastic}}=0$ might result from the terminal electron-phonon coupling at the links, which include thermalized Green's functions instead of Green's function obtained from the kinematic steady-state equations. Owing to the minuteness of the deviation, the heat dissipation in the chain conductor might be negligibly small. The energy exchanged between electrons and phonons via the inelastic coupling between $Q_p^{\mathrm{inelastic}}$ is mostly transported to the p thermalized electrode, and the energy dissipation might occur there. The inelastic energy current $Q_p^{\mathrm{inelastic}}$ appears even in the isothermal case, which is calculated to be about 0.04 pW at $V=0.15$ and becoming larger as λ increases.

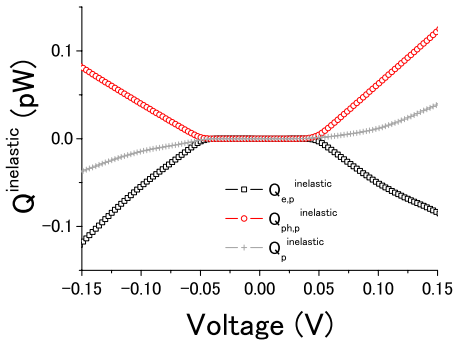

FIG. 10. (Color online) The dependence of the p terminal energy current Q_p on the voltage and the respective contributions from electrons and phonons, i.e., $Q_{e,p}$ and $Q_{\mathrm{ph},p}$ in the isothermal condition, where $k_BT=0.02$($T=23.21$ K). The gray crosses, the open squares, and the open circles denote Q_p, $Q_{e,p}$, and $Q_{\mathrm{ph},p}$, respectively. The units of the voltage and the energy current are given by V and pW, respectively.

B. Transport properties in the nonisothermal case

Here, we provide a brief discussion of the nonisothermal case and introduce two different local temperatures $T_p \neq T_q$ for the two electrodes labeled p and q. Now the temperature gradient becomes finite, i.e., $\nabla \cdot T \neq 0$, and finite thermoelectronic power might appear as a result. The vibronic component of the total electronic current $I_{\mathrm{total}(\Delta)}$ was calculated in two nonisothermal conditions. We studied two cases here, i.e., (ia′) $t=-1.0$, $t_M=-1.0$, $t_L=-1.0$, $\varepsilon=0.5$, $\varepsilon_M=0.0$, $k_C=2.5$, $k_M=2.5$, $k_L=2.5$, $M_C=M_M=1833$, $\lambda=0.1$, $k_BT_p=0.002$, and $k_BT_q=0.02$ and (ia″) $t=-1.0$, $t_M=-1.0$, $t_L=-1.0$, $\varepsilon=0.5$, $\varepsilon_M=0.0$, $k_C=2.5$, $k_M=2.5$, $k_L=2.5$, $M_C=M_M=1833$, $\lambda=0.1$, $k_BT_p=0.02$, and $k_BT_q=0.002$. $T_p=23.21$ K and $T_q=232.1$ K for (ia′) and $T_p=232.1$ K and $T_q=23.21$ K for (ia″), respectively. The calculation results of the vibronic current component, i.e., $I_{\mathrm{total}(\Delta)}=I_{\mathrm{total}}-I_{\mathrm{ballistic}}$, are summarized in Fig. 11. We found two finite intercepts at about $\pm 1\times 10^{-3}$ on the V coordinate in the $I_{\mathrm{total}(\Delta)}-V$ plots. The intercept might appear as a result of the thermoelec-

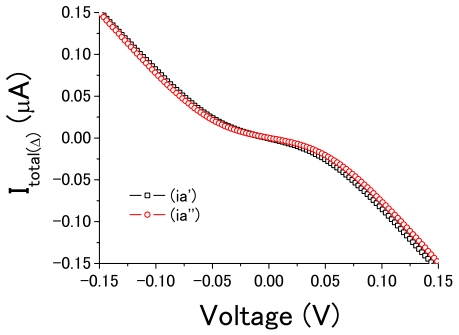

FIG. 11. (Color online) The *I-V* curve of the total electronic current subtracted by the ballistic electronic current, i.e., $I_{\text{total}(\Delta)}=I_{\text{total}}-I_{\text{ballistic}}$ in two nonisothermal conditions, i.e., (ia′) $t=-1.0$, $t_M=-1.0$, $t_L=-1.0$, $\varepsilon=0.5$, $\varepsilon_M=0.0$, $k_C=2.5$, $k_M=2.5$, $k_L=2.5$, $M_C=M_M=1833$, $\lambda=0.5$, and $k_BT_p=0.02$, $k_BT_q=0.002$ and (ia″) $t=-1.0$, $t_M=-1.0$, $t_L=-1.0$, $\varepsilon=0.5$, $\varepsilon_M=0.0$, $k_C=2.5$, $k_M=2.5$, $k_L=2.5$, $M_C=M_M=1833$, $\lambda=0.5$, $k_BT_p=0.002$, and $k_BT_q=0.02$. The units of k_BT are in eV. $k_BT_p=0.02$ and $k_BT_q=0.002$ corresponds to 232.1 K and 23.21 K, respectively. The open squares and the open circles denote the calculation results of $I_{\text{total}(\Delta)}$ for the two cases (ia′) and (ia″), respectively. The units of the voltage and the current are in V and μA.

tronic power,[75,76] which can be estimated in these cases to be -5 μV/K. Whether or not the temperature gradient and the voltage are aligned favorably can produce differences in the $I_{\text{total}(\Delta)}-V$ curve. This might be the reason why we observed different slopes in the plots. It is also interesting to point out that the plots enclose a very thin looplike hysteresis due to these reasons.

IV. DISCUSSION

It was found that in Figs. 7 and 8 the lowest-energy phonon modes whose energies are found to be smaller than 0.02 in Fig. 4 do not play a major role in determining the shape of the plot of d^2I/dV^2 in both the resonant and the tunneling cases. Such phonon modes seem to be inactive for electron scatterings. Owing to this phonon mode propensity rule, nearly ballistic electronic current is possible at very low bias voltage regions. It was also found that in Figs. 6 and 7 the active phonon modes for d^2I/dV^2 are different for the quasiresonant case and the tunneling case, as well as that they are dependent on the electron density of the states in the conductor. The electron density of the states is another important factor which exerts great influence on the phonon mode dependence. Finally, it was found that in Fig. 7 the peak positions of d^2I/dV^2 shift as the force field k_L changes. Although the change is large in the tunneling case, it is relatively small in the resonant case. The reason for this behavior might again be the density of states of electrons and phonons. Due to the large density in the quasiresonant case, there might be many alternative electron and phonon states which can take part in electron-phonon coupling phenomena. On the other hand, in the tunneling case, owing to the sparseness of the electron density of the states, the number of available states might be limited to the energy range around the peak. In this case, we might have larger shifts in the tunneling case.

In addition, we observed a voltage dependence of the offset of d^2I/dV^2. It is important to describe the global features of the *I-V* curve. Recently, the negative differential resistance (NDR) behavior has been recognized in the electron-transport property of suspended carbon nanotubes,[77] and the origin of NDR has been actively discussed. Above all, the nonequilibrium phonon effect has received considerable attention,[78] and it is possible that there is a connection between our theory and this problem. Regarding the coupling constant $\lambda=0.1$ and the studied systems with respective sizes $N_C=3$, 4, and 5, no clear NDR behavior was confirmed. However, the sign change in $d^2I_{\text{total}(\Delta)}/dV^2$ close to the positions of the peaks and dips found in the strongest mechanical coupling case (3) $k_L/k_C=4.0$ in Fig. 7(a), which was discussed in Sec. III A 3, might be an indication of a possible NDR behavior within our theoretical model. Thus, nonequilibrium phonon effects might play an important role in the NDR phenomenon of vibronic coupling origin. In this context, it should be noted that another possibility in the strong-coupling limit, i.e., the polaron model, has been addressed with an emphasis on its hysteresis behavior of the *I-V* curve due to the possible bistable geometric nature of the model.[79] It should also be mentioned that the offset has been investigated extensively by introducing a rate equation for the vibrational occupation number appearing in the lowest-order perturbation theory of the transport.[41–43] The phenomenological arguments provided in the cited literature appear to have sufficient explanatory power, except with regard to the voltage dependence of the offset found here. Attention should also be paid to some differences between the terminology used in our papers and that in other studies, where the strong damped limit utilized by other authors corresponds to the $\Pi_{e\text{-ph}}(E)=0$ case in this paper.

Additionally, the results revealed asymmetry in the voltage dependence of $Q_{e,p}^{\text{inelastic}}$ and $Q_{\text{ph},p}^{\text{inelastic}}$. It plays an important role in keeping the p terminal inelastic energy current $Q_p^{\text{inelastic}}$ finite after the cancellation of the electron and the phonon contributions. The inelastic energy current might be of vibronic nature in this context, and it is possible that asymmetry might be the result of a nonequilibrium phonon effect similar to the phonon drag effect. Here, in the quasiresonant case (ia), electrons are mostly scattered backward from their incidental momentum direction, which gives rise to a suppression of the electronic current. In order to keep the momentum conservation, phonons are scattered forward, which gives rise to asymmetry in both $Q_{e,p}^{\text{inelastic}}$ and $Q_{\text{ph},p}^{\text{inelastic}}$.

Recently, the author noticed the existence of two theoretical papers in the literature which focus on the problem of energy dissipation.[80–82] These are closely related with the $Q_{\text{ph},p}^{\text{inelastic}}$ part of the present work. However, the calculation results in these papers were based on the one-dimensional electrode model. It is well known that the density of states of electrons and phonons at low energies in one dimension are quite different from those in realistic three-dimensional systems. Single-level models[80] are special from the point of view that electron-hole excitations, both real and virtual, are not allowed due to their small Hilbert space. In spite of these unphysical features, as well as some other simplifications

and theoretical differences used in their calculations, some of the general features of their results remain consistent with ours. It should be noted that they have not discussed the electron contribution, i.e., $Q_{e,p}^{\text{inelastic}}$, to the energy current, which indicates that only a part of the problem has been covered. The author believes that the detailed calculation results given here can reinforce their arguments and can provide additional information which has not been discussed in these works.

V. CONCLUSIONS

In this study, we developed a self-consistent theory where both electron transport and energy transport were treated on equal footing. By using this theory, we studied two problems, i.e., (1) the nonequilibrium phonon effect on the electron transport and (2) the inelastic electron-phonon coupling effect on the energy current. With regard to problem (1), we found that the offset of d^2I/dV^2 depends on the voltage, the energy, and the link force field, which is important for characterizing global *I-V* behavior at high voltages. It was found that electron-hole excitations play an important role in determining the offset behavior in resonant electronic systems. In problem (2), we found that the inelastic coupling raised a new vibronic energy current component at finite voltages. The energy current arises even in isothermal conditions due to the incomplete cancellation between local heating (cooling) energies of electrons and phonons, i.e., the inelastic energy balance. The incomplete cancellation is due to the asymmetric voltage dependencies of these quantities, which might result from the nonequilibrium nature of phonons, i.e., an effect similar to the phonon drag effect. As a result, the vibronic energy current is enhanced at the same voltage positions as the peak and the dip of d^2I/dV^2.

ACKNOWLEDGMENTS

The author is deeply indebted to Hidetoshi Fukuyama of Tokyo University of Science and expresses his gratitude for the discussion on the mechanical coupling between the electrode phonons and the conductor vibrations given here. The author also would like to thank Yoshiyasu Matsumoto of Kyoto University for informing the author about some references on surface phonons.

APPENDIX A

The matrix components of the supermatrices on the left-hand side of Eq. (21) are given as follows:

$$\mathbf{K}_0(\vec{Q}_\parallel) = \begin{pmatrix} K_{xx}(0,0;\vec{Q}_\parallel) & K_{xy}(0,0;\vec{Q}_\parallel) & K_{xz}(0,0;\vec{Q}_\parallel) \\ K_{yx}(0,0;\vec{Q}_\parallel) & K_{yy}(0,0;\vec{Q}_\parallel) & K_{yz}(0,0;\vec{Q}_\parallel) \\ K_{zx}(0,0;\vec{Q}_\parallel) & K_{zy}(0,0;\vec{Q}_\parallel) & K_{zz}(0,0;\vec{Q}_\parallel) \end{pmatrix}, \tag{A1}$$

$$\mathbf{K}_+(\vec{Q}_\parallel) = \begin{pmatrix} K_{xx}(0,1;\vec{Q}_\parallel) & K_{xy}(0,1;\vec{Q}_\parallel) & K_{xz}(0,1;\vec{Q}_\parallel) \\ K_{yx}(0,1;\vec{Q}_\parallel) & K_{yy}(0,1;\vec{Q}_\parallel) & K_{yz}(0,1;\vec{Q}_\parallel) \\ K_{zx}(0,1;\vec{Q}_\parallel) & K_{zy}(0,1;\vec{Q}_\parallel) & K_{zz}(0,1;\vec{Q}_\parallel) \end{pmatrix}, \tag{A2}$$

$$\mathbf{K}_-(\vec{Q}_\parallel) = \begin{pmatrix} K_{xx}(0,-1;\vec{Q}_\parallel) & K_{xy}(0,-1;\vec{Q}_\parallel) & K_{xz}(0,-1;\vec{Q}_\parallel) \\ K_{yx}(0,-1;\vec{Q}_\parallel) & K_{yy}(0,-1;\vec{Q}_\parallel) & K_{yz}(0,-1;\vec{Q}_\parallel) \\ K_{zx}(0,-1;\vec{Q}_\parallel) & K_{zy}(0,-1;\vec{Q}_\parallel) & K_{zz}(0,-1;\vec{Q}_\parallel) \end{pmatrix}, \tag{A3}$$

and

$$\mathbf{D}^R_{l_z,l'_z}(\vec{Q}_\parallel,\omega) = \begin{pmatrix} D^R_{xx}(l_z,l'_z;\vec{Q}_\parallel,\omega) & D^R_{xy}(l_z,l'_z;\vec{Q}_\parallel,\omega) & D^R_{xz}(l_z,l'_z;\vec{Q}_\parallel,\omega) \\ D^R_{yx}(l_z,l'_z;\vec{Q}_\parallel,\omega) & D^R_{yy}(l_z,l'_z;\vec{Q}_\parallel,\omega) & D^R_{yz}(l_z,l'_z;\vec{Q}_\parallel,\omega) \\ D^R_{zx}(l_z,l'_z;\vec{Q}_\parallel,\omega) & D^R_{zy}(l_z,l'_z;\vec{Q}_\parallel,\omega) & D^R_{zz}(l_z,l'_z;\vec{Q}_\parallel,\omega) \end{pmatrix}. \tag{A4}$$

We denote the surface layer by $l_z=0$. The nearest neighbors of the surface layer located on the positive branch of the z axis and that on the negative branch are labeled by 1 and -1, respectively. We have assumed that translational symmetry still exists along the z axis, i.e., $K_{\alpha\beta}(l_z,l_z;\vec{Q}_\parallel) = K_{\alpha\beta}(0,0;\vec{Q}_\parallel)$ and $K_{\alpha\beta}(l_z,l_z\pm1;\vec{Q}_\parallel)=K_{\alpha\beta}(0,\pm1;\vec{Q}_\parallel)$, except at the surface layer. The difference at the surface layer is corrected by using a delta function $\delta_{0,\text{surface}}$, which is defined such that $\delta_{0,\text{surface}}$ is equal to 1 when the layer is located at the outmost surface and to 0 otherwise.[59] The details of the matrix elements in the case of (001) semi-infinite fcc lattice are given in Appendix B.

APPENDIX B

For the (001) semi-infinite fcc lattice, the matrix elements of $\mathbf{K}_0(\vec{Q}_\parallel)$ and $\mathbf{K}_\pm(\vec{Q}_\parallel)$ in Eqs. (A1)–(A3) are given by

$$K_{xx}(0,0;\vec{Q}_\parallel) = K_{yy}(0,0;\vec{Q}_\parallel) = \frac{k_M}{2}\left(2-\cos q_x \cos q_y - \frac{1}{2}\delta_{0,\text{surface}}\right),$$

$$K_{xy}(0,0;\vec{Q}_\parallel) = K_{yx}(0,0;\vec{Q}_\parallel) = \frac{k_M}{2}\sin q_x \sin q_y,$$

$$K_{zz}(0,0;\vec{Q}_\parallel) = \frac{k_M}{2}(2 - \delta_{0,\text{surface}}),$$

$$K_{xz}(0,0;\vec{Q}_\parallel) = K_{zx}(0,0;\vec{Q}_\parallel) = K_{yz}(0,0;\vec{Q}_\parallel) = K_{zy}(0,0;\vec{Q}_\parallel) = 0,$$

$$K_{xx}(0,\pm 1;\vec{Q}_\parallel) = -\frac{k_M}{2}\cos q_x,$$

$$K_{yy}(0,\pm 1;\vec{Q}_\parallel) = -\frac{k_M}{2}\cos q_y,$$

$$K_{zz}(0,\pm 1;\vec{Q}_\parallel) = -\frac{k_M}{2}(\cos q_x + \cos q_y),$$

$$K_{xz}(0,\pm 1;\vec{Q}_\parallel) = K_{zx}(0,\pm 1;\vec{Q}_\parallel) = -\frac{k_M}{2}\cdot(\pm i)\sin q_x,$$

$$K_{yz}(0,\pm 1;\vec{Q}_\parallel) = K_{zy}(0,\pm 1;\vec{Q}_\parallel) = -\frac{k_M}{2}\cdot(\pm i)\sin q_y,$$

$$K_{xy}(0,\pm 1;\vec{Q}_\parallel) = K_{yx}(0,\pm 1;\vec{Q}_\parallel) = 0,$$

where $q_{x(y)} = \frac{Q_{x(y)}a_M}{2}$. We have studied the fcc lattice since the off-diagonal elements disappear in simpler lattices, such as the simple-cubic (sc) lattice, within the nearest-neighbor approximation. This makes the local density of states of phonons in the (sc) lattice thus calculated appears as a one-dimensional one, which is avoided in the fcc lattice.

APPENDIX C

The matrix components of the supermatrices on the left-hand side of Eq. (29) are given as follows:

$$\mathbf{K}_M = \begin{pmatrix} \mathbf{K}_0(\vec{Q}_\parallel) & \mathbf{K}_+(\vec{Q}_\parallel) & \mathbf{0} & \cdots \\ \mathbf{K}_-(\vec{Q}_\parallel) & \mathbf{K}_0(\vec{Q}_\parallel) & \mathbf{K}_+(\vec{Q}_\parallel) & \cdots \\ \mathbf{0} & & \ddots & \\ \vdots & & & \end{pmatrix}, \tag{C1}$$

$$\mathbf{K}_C = \begin{pmatrix} \mathbf{K}_{m,0} & \mathbf{K}_{m,+} & \mathbf{0} & \cdots \\ \mathbf{K}_{m,-} & \mathbf{K}_{m,0} & \mathbf{K}_{m,+} & \cdots \\ \mathbf{0} & & \ddots & \\ \vdots & & & \mathbf{K}_{m,0} \end{pmatrix}, \tag{C2}$$

$$\mathbf{K}_{L+} = \begin{pmatrix} \mathbf{0} & \cdots & & \mathbf{0} \\ \mathbf{0} & \mathbf{0} & & \mathbf{0} \\ \vdots & & \ddots & \vdots \\ \mathbf{K}_{m,+} & \cdots & & \mathbf{0} \end{pmatrix}, \tag{C3}$$

$$\mathbf{K}_{L-} = \begin{pmatrix} \mathbf{0} & \cdots & & \mathbf{K}_{m,-} \\ \mathbf{0} & \mathbf{0} & & \mathbf{0} \\ \vdots & & \ddots & \vdots \\ \mathbf{0} & \cdots & & \mathbf{0} \end{pmatrix}, \tag{C4}$$

$$\mathbf{K}_{m,0} = \begin{pmatrix} 0 & 0 & 0 \\ 0 & 0 & 0 \\ 0 & 0 & K_{zz}(0,0) \end{pmatrix}, \tag{C5}$$

$$\mathbf{K}_{m,+} = \begin{pmatrix} 0 & 0 & 0 \\ 0 & 0 & 0 \\ 0 & 0 & K_{zz}(0,1) \end{pmatrix}, \tag{C6}$$

and

$$\mathbf{K}_{m,-} = \begin{pmatrix} 0 & 0 & 0 \\ 0 & 0 & 0 \\ 0 & 0 & K_{zz}(0,-1) \end{pmatrix}, \tag{C7}$$

where 0 and ± 1 denote $R_z = 0$ and $R_z = \pm 1$. We have ignored the x and y components of $\vec{R}$ in $K_{zz}(\vec{R}_i;\vec{R}_j)$ since the chain conductor is aligned along the z axis.

APPENDIX D

The matrix element of the electronic link Hamiltonians, i.e., $\mathbf{H}_{L+}$ and $\mathbf{H}_{L-}$ are given below,

$$\mathbf{H}_{L+} = \begin{pmatrix} 0 & \cdots & \cdots & 0 \\ \vdots & \ddots & & \vdots \\ 0 & & \ddots & \vdots \\ t_L & 0 & \cdots & 0 \end{pmatrix}, \tag{D1}$$

and

$$\mathbf{H}_{L-} = \begin{pmatrix} 0 & \cdots & 0 & t_L \\ \vdots & \ddots & & 0 \\ \vdots & & \ddots & \vdots \\ 0 & \cdots & \cdots & 0 \end{pmatrix}. \tag{D2}$$

APPENDIX E

In this appendix, we discuss the approximate relation $Q_{e,\text{exch}} + Q_{\text{ph,exch}} \simeq 0$, which has been suggested in more simple models.[80] We use the Born and bubble approximations under the steady-state condition. By definition,

$$Q_{\text{ph,exch}} = \frac{1}{h}\sum_\sigma \int_{-\infty}^{\infty} E \cdot \text{Tr}[\Pi^<_{e\text{-ph},\sigma}(E)\mathbf{D}^>_C(E) - \Pi^>_{e\text{-ph},\sigma}(E)\mathbf{D}^<_C(E)]dE,$$

and

$$Q_{e,\text{exch}} = -\frac{2}{h}\int_{-\infty}^{\infty} E \cdot \text{Tr}[\mathbf{\Sigma}^>_{e\text{-ph}}(E)\mathbf{G}^<_C(E) - \mathbf{\Sigma}^<_{e\text{-ph}}(E)\mathbf{G}^>_C(E)]dE.$$

Taking into account Eq. (68), $Q_{\text{ph,exch}}$ can be rewritten as follows:

$$Q_{\mathrm{ph,exch}} = \frac{2}{h} \cdot \frac{i\lambda^2 t_L^2}{M_C} \sum_{i,j} \sum_{\delta_1,\delta_2,\delta_3,\delta_4} \mathrm{sgn}_{\delta_1,\delta_2,\delta_3,\delta_4} \int_{-\infty}^{\infty} \int_{-\infty}^{\infty} E\{G^<_{C_{i+\delta_1,j+\delta_2}}(\Lambda) G^>_{C_{j+\delta_3,i+\delta_4}}(\Lambda - E) D^>_{C_{j,i}}(E)$$
$$- G^>_{C_{i+\delta_1,j+\delta_2}}(\Lambda) G^<_{C_{j+\delta_3,i+\delta_4}}(\Lambda - E) D^<_{C_{j,i}}(E)\} dE d\Lambda$$

Similarly, if we refer to Eq. (65), $Q_{e,\mathrm{exch}}$ is given by

$$Q_{e,\mathrm{exch}} = -\frac{2}{h} \cdot \frac{i\lambda^2 t_L^2}{M_C} \sum_{i,j} \sum_{\langle \delta_1,\delta_2,\delta_3,\delta_4 \rangle} \mathrm{sgn}'_{\delta_1,\delta_2,\delta_3,\delta_4} \int_{-\infty}^{\infty} \int_{-\infty}^{\infty} E\{G^>_{C_{i+\delta_1,j+\delta_2}}(\Lambda - E) D^>_{C_{i+\delta_4,j+\delta_3}}(E) G^<_{C_{j,i}}(\Lambda)$$
$$- G^<_{C_{i+\delta_1,j+\delta_2}}(\Lambda - E) D^<_{C_{i+\delta_4,j+\delta_3}}(E) G^>_{C_{j,i}}(\Lambda)\} dE d\Lambda$$
$$= -\frac{2}{h} \cdot \frac{i\lambda^2 t_L^2}{M_C} \sum_{i',j'} \sum_{\langle \delta'_1,\delta'_2,\delta'_3,\delta'_4 \rangle} \mathrm{sgn}'_{\delta'_1,\delta'_2,\delta'_3,\delta'_4} \int_{-\infty}^{\infty} \int_{-\infty}^{\infty} E\{G^<_{C_{i'+\delta'_1,j'+\delta'_2}}(\Lambda) G^>_{C_{j'+\delta'_3,i'+\delta'_4}}(\Lambda - E) D^>_{C_{j',i'}}(E)$$
$$- G^>_{C_{i'+\delta'_1,j'+\delta'_2}}(\Lambda) G^<_{C_{j'+\delta'_3,i'+\delta'_4}}(\Lambda - E) D^<_{C_{j',i'}}(E)\} dE d\Lambda$$

The sum over the displacements $\langle \delta_1, \delta_2, \delta_3, \delta_4 \rangle$ and the signs $\mathrm{sgn}_{\delta_1,\delta_2,\delta_3,\delta_4}$ and $\mathrm{sgn}'_{\delta_1,\delta_2,\delta_3,\delta_4}$ represent the signed sum given in the Appendixes F and G. We can write $\mathrm{sgn}_{\delta_1,\delta_2,\delta_3,\delta_4} = \mathrm{sgn}'_{\delta'_1,\delta'_2,\delta'_3,\delta'_4}$ since both terms have the same origin, i.e., the signs of the cross terms of the product $(u_{i+1z} - u_{iz}) \cdot (u_{j+1z} - u_{jz})$. Therefore, within the steady-state approximation, $Q_{e,\mathrm{exch}} + Q_{\mathrm{ph,exch}} \simeq 0$. $Q^{\mathrm{inelastic}}_{e,p}$ and $Q^{\mathrm{inelastic}}_{\mathrm{ph},p}$, given in Eqs. (74c) and (75c), can be rewritten as follows:

$$Q^{\mathrm{inelastic}}_{e,p} = -\frac{2}{h} \int_{-\infty}^{\infty} E \cdot \mathrm{Tr}[\boldsymbol{\Sigma}^>_p(E) \mathbf{G}^R_C(E) \boldsymbol{\Sigma}^<_{e\text{-ph}}(E) \mathbf{G}^A_C(E)$$
$$- \boldsymbol{\Sigma}^<_p(E) \mathbf{G}^R_C(E) \boldsymbol{\Sigma}^>_{e\text{-ph}}(E) \mathbf{G}^A_C(E)] dE,$$

$$Q^{\mathrm{inelastic}}_{\mathrm{ph},p} = \frac{1}{h} \int_{-\infty}^{\infty} E \cdot \mathrm{Tr}[\boldsymbol{\Pi}^<_p(E) \mathbf{D}^R_C(E) \boldsymbol{\Pi}^>_{e\text{-ph}}(E) \mathbf{D}^A_C(E)$$
$$- \boldsymbol{\Pi}^>_p(E) \mathbf{D}^R_C(E) \boldsymbol{\Pi}^<_{e\text{-ph}}(E) \mathbf{D}^A_C(E)] dE.$$

In this form, it is clear that $Q^{\mathrm{inelastic}}_{e,p} + Q^{\mathrm{inelastic}}_{e,q} = -Q_{e,\mathrm{exch}}$ and $Q^{\mathrm{inelastic}}_{\mathrm{ph},p} + Q^{\mathrm{inelastic}}_{\mathrm{ph},q} = -Q_{\mathrm{ph,exch}}$. Then, $Q^{\mathrm{inelastic}}_{e,p} + Q^{\mathrm{inelastic}}_{e,q} + Q_{e,\mathrm{exch}} + Q_{\mathrm{ph,exch}} = 0$ rigorously. Therefore, $Q^{\mathrm{inelastic}}_p + Q^{\mathrm{inelastic}}_q \simeq 0$ within the approximation, where $Q^{\mathrm{inelastic}}_p = Q^{\mathrm{inelastic}}_{e,p} + Q^{\mathrm{inelastic}}_{\mathrm{ph},p}$. In the two-terminal systems composed of p and q, $Q^{\mathrm{elastic}}_{e,p}$ and $Q^{\mathrm{elastic}}_{\mathrm{ph},p}$ given in Eqs. (74b) and (75b) are simplified to

$$Q^{\mathrm{elastic}}_{e,p} = -\frac{2}{h} \int_{-\infty}^{\infty} E \cdot \bar{T}_e(E) \{f_q(E) - f_p(E)\} dE,$$

$$Q^{\mathrm{elastic}}_{\mathrm{ph},p} = \frac{1}{h} \int_{-\infty}^{\infty} E \cdot \bar{T}_{\mathrm{ph}}(E) \{b_q(E) - b_p(E)\} dE.$$

Then, $Q^{\mathrm{elastic}}_{e,p} + Q^{\mathrm{elastic}}_{e,q} = 0$ and $Q^{\mathrm{elastic}}_{\mathrm{ph},p} + Q^{\mathrm{elastic}}_{\mathrm{ph},q} = 0$ rigorously, and thus, $Q^{\mathrm{elastic}}_p + Q^{\mathrm{elastic}}_q = 0$. As a result, $Q_p + Q_q \simeq 0$ within the approximation, where $Q_{p(q)} = Q^{\mathrm{elastic}}_{p(q)} + Q^{\mathrm{inelastic}}_{p(q)}$. It should be noted that the following relation is satisfied exactly: $Q_p + Q_q + Q_{e,\mathrm{exch}} + Q_{\mathrm{ph,exch}} = 0$.

APPENDIX F

The second-order chronological e-ph self-energy of electrons $\Sigma^t_{e\text{-ph}}(i,t_1;j,t_2)$ was calculated in real coordinate space. The calculation results have been summarized as follows:

$$\Sigma^t_{e\text{-ph}}(i,t_1;j,t_2) = i\lambda^2 t_L^2 G^t(i-1,t_1;j+1,t_2)\tilde{D}^t(i,t_1;j+1,t_2) + i\lambda^2 t_L^2 G^t(i-1,t_1;j+1,t_2)\tilde{D}^t(i-1,t_1;j,t_2) - i\lambda^2 t_L^2 G^t(i-1,t_1;j+1,t_2)\tilde{D}^t(i-1,t_1;j+1,t_2) - i\lambda^2 t_L^2 G^t(i-1,t_1;j+1,t_2)\tilde{D}^t(i,t_1;j,t_2) + i\lambda^2 t_L^2 G^t(i-1,t_1;j-1,t_2)\tilde{D}^t(i,t_1;j,t_2) + i\lambda^2 t_L^2 G^t(i-1,t_1;j-1,t_2)\tilde{D}^t(i-1,t_1;j-1,t_2) - i\lambda^2 t_L^2 G^t(i-1,t_1;j-1,t_2)\tilde{D}^t(i-1,t_1;j,t_2) - i\lambda^2 t_L^2 G^t(i-1,t_1;j-1,t_2)\tilde{D}^t(i,t_1;j-1,t_2) + i\lambda^2 t_L^2 G^t(i+1,t_1;j+1,t_2)\tilde{D}^t(i+1,t_1;j+1,t_2) + i\lambda^2 t_L^2 G^t(i+1,t_1;j+1,t_2)\tilde{D}^t(i,t_1;j,t_2) - i\lambda^2 t_L^2 G^t(i+1,t_1;j+1,t_2)\tilde{D}^t(i,t_1;j+1,t_2) - i\lambda^2 t_L^2 G^t(i+1,t_1;j+1,t_2)\tilde{D}^t(i+1,t_1;j,t_2) + i\lambda^2 t_L^2 G^t(i+1,t_1;j-1,t_2)\tilde{D}^t(i+1,t_1;j,t_2) + i\lambda^2 t_L^2 G^t(i+1,t_1;j-1,t_2)\tilde{D}^t(i,t_1;j-1,t_2) - i\lambda^2 t_L^2 G^t(i+1,t_1;j-1,t_2)\tilde{D}^t(i,t_1;j,t_2) - i\lambda^2 t_L^2 G^t(i+1,t_1;j-1,t_2)\tilde{D}^t(i+1,t_1;j-1,t_2),$$

where $iG^t(i,t_1;j,t_2) \equiv \langle T[c_i(t_1)c^\dagger_j(t_2)] \rangle_0$ and $i\tilde{D}^t(i,t_1;j,t_2) \equiv \langle T[u_i(t_1)u_j(t_2)] \rangle_0$.

APPENDIX G

The second-order chronological e-ph self-energy of phonons $\Pi^t_{e\text{-ph},\sigma}(i,t_1;j,t_2)$ given by the lowest bubble diagram was calculated in the real coordinate space. The calculation results have been summarized as follows:

$$\begin{aligned}\Pi^t_{e\text{-ph},\sigma}(i,t_1;j,t_2) = {} & i\frac{\lambda^2 t_L^2}{M_C}G^t_\sigma(i-1,t_1;j,t_2)G^t_\sigma(j-1,t_2;i,t_1) + i\frac{\lambda^2 t_L^2}{M_C}G^t_\sigma(i-1,t_1;j-1,t_2)G^t_\sigma(j,t_2;i,t_1) + i\frac{\lambda^2 t_L^2}{M_C}G^t_\sigma(i,t_1;j,t_2)G^t_\sigma(j \\ & -1,t_2;i-1,t_1) + i\frac{\lambda^2 t_L^2}{M_C}G^t_\sigma(i,t_1;j-1,t_2)G^t_\sigma(j,t_2;i-1,t_1) + i\frac{\lambda^2 t_L^2}{M_C}G^t_\sigma(i,t_1;j+1,t_2)G^t_\sigma(j,t_2;i+1,t_1) \\ & + i\frac{\lambda^2 t_L^2}{M_C}G^t_\sigma(i,t_1;j,t_2)G^t_\sigma(j+1,t_2;i+1,t_1) + i\frac{\lambda^2 t_L^2}{M_C}G^t_\sigma(i+1,t_1;j+1,t_2)G^t_\sigma(j,t_2;i,t_1) + i\frac{\lambda^2 t_L^2}{M_C}G^t_\sigma(i+1,t_1;j,t_2)G^t_\sigma(j \\ & +1,t_2;i,t_1) - i\frac{\lambda^2 t_L^2}{M_C}G^t_\sigma(i,t_1;j,t_2)G^t_\sigma(j-1,t_2;i+1,t_1) - i\frac{\lambda^2 t_L^2}{M_C}G^t_\sigma(i,t_1;j-1,t_2)G^t_\sigma(j,t_2;i+1,t_1) - i\frac{\lambda^2 t_L^2}{M_C}G^t_\sigma(i \\ & +1,t_1;j,t_2)G^t_\sigma(j-1,t_2;i,t_1) - i\frac{\lambda^2 t_L^2}{M_C}G^t_\sigma(i+1,t_1;j-1,t_2)G^t_\sigma(j,t_2;i,t_1) - i\frac{\lambda^2 t_L^2}{M_C}G^t_\sigma(i-1,t_1;j \\ & +1,t_2)G^t_\sigma(j,t_2;i,t_1) - i\frac{\lambda^2 t_L^2}{M_C}G^t_\sigma(i-1,t_1;j,t_2)G^t_\sigma(j+1,t_2;i,t_1) - i\frac{\lambda^2 t_L^2}{M_C}G^t_\sigma(i,t_1;j+1,t_2)G^t_\sigma(j,t_2;i-1,t_1) \\ & - i\frac{\lambda^2 t_L^2}{M_C}G^t_\sigma(i,t_1;j,t_2)G^t_\sigma(j+1,t_2;i-1,t_1)\end{aligned}$$

[1] S. Datta, *Electronic Transport in Mesoscopic Systems* (Cambridge University Press, Cambridge, 1995).
[2] D. K. Ferry and S. M. Goodnick, *Transport in Nanostructure* (Cambridge University Press, Cambridge, 1997).
[3] A. Aviram and M. A. Ratner, Chem. Phys. Lett. **29**, 277 (1974).
[4] M. A. Reed and J. M. Tour, Sci. Am. **282**(6), 86 (2000).
[5] Special issue on Transport in Molecular Wires, edited by P. Hänggi, M. Ratner, and S. Yaliraki, Chem. Phys. **281**, Issue 2-3 (2002).
[6] J. R. Heath and M. A. Ratner, Phys. Today **56**(5), 43 (2003).
[7] A. S. Alexandrov, J. Demsar, and E. I. K. Yanson, *Molecular Nanowires and Other Quantum Objects* (Kluwer, Dordrecht, 2004).
[8] G. Curiberti, G. Fagas, and K. Richter, *Introducing Molecular Electronics* (Springer-Verlag, Berlin, 2005).
[9] V. Mujica, M. Kemp, and M. A. Ratner, J. Chem. Phys. **101**, 6856 (1994).
[10] E. G. Emberly and G. Kirczenow, Phys. Rev. B **62**, 10451 (2000).
[11] Y. Asai and H. Fukuyama, Phys. Rev. B **72**, 085431 (2005).
[12] N. D. Lang, Phys. Rev. B **52**, 5335 (1995).
[13] M. Di Ventra, S. T. Pantelides, and N. D. Lang, Phys. Rev. Lett. **84**, 979 (2000).
[14] J. Taylor, H. Guo, and J. Wang, Phys. Rev. B **63**, 121104(R) (2001).
[15] M. Brandbyge, J.-L. Mozos, P. Ordejón, J. Taylor, and K. Stokbro, Phys. Rev. B **65**, 165401 (2002).
[16] T. Rakshit, G.-C. Liang, A. W. Ghosh, M. C. Hersam, and S. Datta, Phys. Rev. B **72**, 125305 (2005).
[17] W. Ho, J. Chem. Phys. **117**, 11033 (2002).
[18] N. Agraït, C. Untiedt, G. Rubio-Bollinger, and S. Vieira, Phys. Rev. Lett. **88**, 216803 (2002).
[19] R. H. M. Smit, Y. Noat, C. Untiedt, N. D. Lang, M. C. van Hemert, and J. M. van Ruitenbeek, Nature (London) **419**, 906 (2002).
[20] D. Djukic, K. S. Thygesen, C. Untiedt, R. H. M. Smit, K. W. Jacobsen, and J. M. van Ruitenbeek, Phys. Rev. B **71**, 161402(R) (2005).
[21] M. Kiguchi, R. Stadler, I. S. Kristensen, D. Djukic, and J. M. van Ruitenbeek, Phys. Rev. Lett. **98**, 146802 (2007).
[22] J. G. Kushmerick, J. Lazorcik, C. H. Patterson, R. Shashidhar, D. S. Seferos, and G. C. Bazan, Nano Lett. **4**, 639 (2004).
[23] L. H. Yu, C. D. Zangmeister, and J. G. Kushmerick, Phys. Rev. Lett. **98**, 206803 (2007).
[24] Y. Sainoo, Y. Kim, T. Okawa, T. Komeda, H. Shigekawa, and M. Kawai, Phys. Rev. Lett. **95**, 246102 (2005).
[25] H. Ness, J. Phys.: Condens. Matter **18**, 6307 (2006).
[26] M. Galperin, M. A. Ratner, and A. Nitzan, J. Phys.: Condens. Matter **19**, 103201 (2007).
[27] A. Troisi, J. M. Beebe, L. B. Picraux, R. D. van Zee, D. R. Stewart, M. A. Ratner, and J. G. Kushmerick, Proc. Natl. Acad. Sci. U.S.A. **104**, 14255 (2007).
[28] Y. Asai and T. Shimazaki, in *Charge Migration in DNA; Physics, Chemistry, and Biology Perspectives*, edited by T. Chakraborty (Springer-Verlag, Berlin, 2007).
[29] C. Caroli, R. Combescot, P. Nozieres, and D. Saint-James, J. Phys. C **5**, 21 (1972).
[30] B. N. J. Persson and A. Baratoff, Phys. Rev. Lett. **59**, 339 (1987).
[31] R. Lake and S. Datta, Phys. Rev. B **46**, 4757 (1992).
[32] H. Ness and A. J. Fisher, Phys. Rev. Lett. **83**, 452 (1999).
[33] N. Mingo and K. Makoshi, Phys. Rev. Lett. **84**, 3694 (2000).
[34] E. G. Emberly and G. Kirczenow, Phys. Rev. B **61**, 5740 (2000).
[35] S. Datta, Nanotechnology **15**, S433 (2004).
[36] T. Yamamoto, K. Watanabe, and S. Watanabe, Phys. Rev. Lett. **95**, 065501 (2005).
[37] A. P. Horsfield, D. R. Bowler, H. Ness, C. G. Sanchez, T. N. Todorov, and A. J. Fisher, Rep. Prog. Phys. **69**, 1195 (2006).
[38] Y. C. Chen, M. Zwolak, and M. Di Ventra, Nano Lett. **4**, 1709 (2004).
[39] Y. Asai, Phys. Rev. Lett. **93**, 246102 (2004); **94**, 099901(E) (2005).
[40] T. Frederiksen, M. Brandbyge, N. Lorente, and A. P. Jauho, Phys. Rev. Lett. **93**, 256601 (2004).

[41] M. Paulsson, T. Frederiksen, and M. Brandbyge, Phys. Rev. B **72**, 201101(R) (2005).
[42] T. Frederiksen, N. Lorente, M. Paulsson, and M. Brandbyge, Phys. Rev. B **75**, 235441 (2007).
[43] T. Frederiksen, M. Paulsson, M. Brandbyge, and A.-P. Jauho, Phys. Rev. B **75**, 205413 (2007).
[44] N. Sergueev, D. Roubtsov, and H. Guo, Phys. Rev. Lett. **95**, 146803 (2005).
[45] N. Sergueev, A. A. Demkov, and H. Guo, Phys. Rev. B **75**, 233418 (2007).
[46] T. Shimazaki and Y. Asai, Phys. Rev. B **77**, 075110 (2008).
[47] A. Troisi and M. A. Ratner, Phys. Rev. B **72**, 033408 (2005).
[48] M. Paulsson, T. Frederiksen, and M. Brandbyge, Nano Lett. **6**, 258 (2006).
[49] M. Galperin, M. A. Ratner, and A. Nitzan, J. Chem. Phys. **121**, 11965 (2004).
[50] J. K. Viljas, J. C. Cuevas, F. Pauly, and M. Häfner, Phys. Rev. B **72**, 245415 (2005).
[51] H. Ueba, T. Mii, and S. G. Tikhodeev, Surf. Sci. **601**, 5220 (2007).
[52] T. Shimazaki and Y. Asai, Phys. Rev. B **77**, 115428 (2008).
[53] The author of this paper recently noticed the existence of two closely related works in the literature. While simpler models have been used in those works, some of the conclusions are similar to the ones presented here. Comments on them will be given in Sec. IV.
[54] A. J. Heeger, S. Kivelson, and J. R. Schrieffer, Rev. Mod. Phys. **60**, 781 (1988).
[55] A. A. Maradudin, E. W. Montroll, and G. H. Weiss, in *Theory of Lattice Dynamics in the Harmonic Approximation*, Solid State Physics Suppl. 3, edited by F. Seitz and D. Turnbull (Academic, New York, 1963).
[56] A. N. Cleland, *Foundations of Nanomechanics: From Solid-State Theory to Device Applications* (Springer, Berlin, 2003).
[57] S. W. Lovesey, *Condensed Matter Physics: Dynamic Correlations* (Benjamin, London, 1980).
[58] *Surface Phonons*, edited by W. Kress and F. W. de Wette (Springer, Berlin, 1991).
[59] H. Ibach and D. L. Mills, *Electron Energy Loss Spectroscopy and Surface Vibrations* (Academic, New York, 1992).
[60] M. P. L. Sancho, J. M. L. Sancho, and J. Rubio, J. Phys. F: Met. Phys. **15**, 851 (1985).
[61] M. B. Nardelli, Phys. Rev. B **60**, 7828 (1999).
[62] G. D. Mahan, *Many-Particle Physics*, 3rd ed. (Kluwer, Dordrecht/Plenum, New York, 2000).
[63] L. P. Kadnoff and G. Baym, *Quantum Statistical Mechanics* (Benjamin, London, 1962).
[64] L. G. C. Rego and G. Kirczenow, Phys. Rev. Lett. **81**, 232 (1998).
[65] D. E. Angelescu, M. C. Cross, and M. L. Roukes, Superlattices Microstruct. **23**, 673 (1998).
[66] N. Mingo and L. Yang, Phys. Rev. B **68**, 245406 (2003).
[67] T. Yamamoto and K. Watanabe, Phys. Rev. Lett. **96**, 255503 (2006).
[68] D. C. Langreth, *Lenear and Nonlinear Electron Transport in Solids* (Plenum, New York, 1976).
[69] A. A. Abrikosov, L. P. Gorkov, and I. E. Dzyaloshinski, *Methods of Quantum Field Theory in Statistical Physics* (Dover, New York, 1975).
[70] A. L. Fetter and J. D. Walecka, *Quantum Theory of Many-Particle Systems* (McGraw-Hill, New York, 1971).
[71] L. Y. Gorelik, A. Isacsson, M. V. Voinova, B. Kasemo, R. I. Shekhter, and M. Jonson, Phys. Rev. Lett. **80**, 4526 (1998).
[72] H. Park, J. Park, A. K. L. Lim, E. H. Anderson, A. P. Alivisatos, and P. L. McEuen, Nature (London) **407**, 57 (2000).
[73] T. Novotny, A. Donarini, C. Flindt, and A.-P. Jauho, Phys. Rev. Lett. **92**, 248302 (2004).
[74] G. A. Kaat and K. Flensberg, Phys. Rev. B **71**, 155408 (2005).
[75] P. Reddy, S.-Y. Jang, R. A. Segalman, and A. Majumdar, Science **315**, 1568 (2007).
[76] M. Paulsson and S. Datta, Phys. Rev. B **67**, 241403(R) (2003).
[77] E. Pop, D. Mann, J. Cao, Q. Wang, K. Goodson, and H. Dai, Phys. Rev. Lett. **95**, 155505 (2005).
[78] C. Auer, F. Schürrer, and C. Ertler, Phys. Rev. B **74**, 165409 (2006).
[79] M. Galperin, M. A. Ratner, A. Nitzan, and A. Troisi, Science **319**, 1056 (2008).
[80] J. T. Lü and J.-S. Wang, Phys. Rev. B **76**, 165418 (2007).
[81] J.-S. Wang, N. Zeng, J. Wang, and C. K. Gan, Phys. Rev. E **75**, 061128 (2007).
[82] E. J. McEniry, D. R. Bowler, D. Dundas, A. P. Horsfield, C. G. Sanchez, and T. N. Todorov, J. Phys.: Condens. Matter **19**, 196201 (2007).